UNIVERSITY OF Hull

Control of Metal-Organic Framework (MOF) Crystal Alignment and

Orientation by Electric Field

Being a Thesis submitted for the degree of

Master of Science by Research

in the University of Hull

Faculty of Science and Engineering

Department of Physics and Mathematics

By

Connor Harry Hall, BSc (Hons)

August 2020

Abstract

Due to most Metal-Organic Frameworks (MOFs) possessing anisotropic properties, it could prove extremely useful to control and manipulate their alignment and orientation. Such control of MOF crystal microrods has previously been demonstrated by use of a magnetic field as part of a collaboration between the University of Hull (UK), University of Vienna (Austria) and Northwestern University (USA). Following on this work, here we show that similar methods can be exploited in order to dynamically align MOF crystals NU-1000 by applying an electric field, making it directly compatible with device integration. Experiments have been performed on this MOF in the form of two different samples: i) an unfixed suspension in bromobenzene allowing for dynamic and reconfigurable alignment and ii) a solid sample with the MOF alignment fixed in place by resin curing. The alignment of the NU-1000 was then confirmed and quantified by studying the fluorescence emission under polarised excitation, taking advantage of the absorption anisotropy. A laser emitting light of wavelength 405nm was used to excite the samples and the resulting fluorescence was measured as a function of the incident angle of polarisation relative to the orientation of the NU-1000 crystal. In a second stage, the emission and absorption polarisation properties of the aligned MOF samples were measured. It was found that the fluorescence emission, as well as the absorption, are polarised along the MOF crystal long axis. This work and potential future work has applications in optics and electronics such as energy transfer, gas sensing and separation, display technology and optical switches.

Contents

Table of Figures

Abbreviations and Symbols

MOF	Metal-Organic Framework
DOT	2,5-dioxidoterephthalate
OMS	Open Metal Site
TDA	4,4-[1,4-phenylenebis-(carbonylimino)]
ODA	4,4-[oxalylbis(imino)]
TGA Curve	Thermogravimetric Analysis Curve
LIB	Lithium-Ion Battery
SIB	Sodium-Ion Battery
NB	4-nitrobenzaldehyde
FDE	4-formyldiphenyl ether
MeOH	Methanol
H_4TBAPy	Tetratopic pyrene-based linker
3-MePent (C_6H_{14})	3-Methylpentane
MeCN (CH_3CN)	Acetonitrile
AN	Acceptor Number
NMR	Nuclear magnetic resonance
BrPh	Bromobenzene (Solvent)
BzOH	Benzoic acid
DMF	N,N-dimethylformamide
TMODS	Trimethoxy(octadecyl)silane
UV	Ultraviolet
CCD	Charged Coupled Device
E	Energy (photon)
h	Planck's Constant
f	Frequency
λ	Wavelength

S_n/V_n	nth singlet/vibrational state
p	Dipole Moment
q	Charge
d	Separation Distance
z	Aspect Ratio
r_a/r_b	Semi-major Axis/Semi-minor Axis
F	Force
E	Electric Field Strength
τ	Torque
μ_e	Extinction Coefficient
$\Psi_{i/f}$	Initial/final State Wavefunction
μ	Dipole Moment Operator
ℓ	Quantum Number

Acknowledgements

I would like to express my appreciation to my supervisor, Dr Jean-Sebastien Bouillard, for his continuous support, guidance and encouragement throughout my studies. His assistance and patience have proved to be invaluable.

I am grateful to Dr Ali Adawi and Dr Neil Kemp for allowing the use of the nanophononics lab and associated equipment and for their supportive input.

I am particularly appreciative to Dr Jia Min Chin and Dr Fei Cheng for their superior assistance in data collection, supply of samples and extensive knowledge from a chemistry perspective. I thank Adam Young likewise.

Without the funding for course, accommodation and living fees provided by Student Finance England, it would not have been possible for me to complete my studies. I am forever grateful for their support and providing me with the chance to experience such opportunities.

I would finally like to thank all my family and friends who have been eternally encouraging and supporting and have helped keep me enthusiastic and optimistic through everything.

1 Introduction

With the relatively new concept of MOFs (Metal Organic Frameworks) continuing to be of rapidly increasing interest within the scientific community, there is an abundance of research potential associated with new MOF properties and applications are being discovered frequently, ranging from gas capture and storage to catalysis.

The aim of the research presented in this thesis is to achieve control of the orientation and alignment of MOFs. The orientation of MOFs has previously been studied by methods including control of growth in different solutions and on different substrates as conducted by Ohhashi et al. 2017[1] and Falcaro et al. 2014[2] respectively as well as multiple layered MOF-on-MOF oriented growth as conducted by Ikigaki et al. 2019[3]. We control the orientation of pre-synthesised MOFs suspended in a solvent by means of an applied external electric field. Similar research conducted by Cheng et al. 2017[4] demonstrated the control of MOF orientation by an applied magnetic field. Similar methods will be used throughout this thesis, with magnetic and electric field alignment and orientation of liquid and resin samples.

The ability to manipulate MOFs in such a way can provide many new, exciting application possibilities that are directly compatible with electronic devices, such as switchable electronic devices and uses in sensor and optical systems.

1.1 Thesis Aims and Outline

The aim of this thesis is to explore the possibility of actively controlling the orientation and fluorescence of metal-organic frameworks. This has been explored

using an externally applied electric field. We use a 405nm laser to excite the MOF and are able to use the polarised excitation luminescence as a measure to determine MOF orientation due to the absorption dipole being along the long axis of the MOF. By making minor alterations to the setup, we also aimed to determine if there is a contrast in the measured fluorescence depending on whether the initial laser beam prior to the sample is polarised or the fluorescence beam after the sample is polarised, as well as any preferential polarisation between aligned and unaligned MOF samples.

This thesis consists of five chapters. Chapter 1 completes by discussing a brief history of MOFs, including their introduction, current applications and future potential.

Chapter 2 contains the literature review for the thesis and covers excitation, emission, fluorescence, dipoles and polarisation. It includes details about the general MOF structure and some current examples and applications, such as the use of Mg-MOF-74, M-MOF-I, M-MOF-II, MIL-53 and Cu-MOF-74 in gas capture, gas sensing, energy storage and catalysis respectively. It also explains the structure and properties of NU-1000, the MOF used in our work, including current applications and why this was the MOF of our choice. Key emission and absorption spectra for the ligand, MOF and solvent are included and how each of these aspects have an effect on results.

Chapter 3 explains the methodology behind the experimentation. It includes the experimental set-ups and reasoning behind the use of them as well as the synthesis process for NU-1000, including synthesis of the ligand H_4TBAPy and further synthesis to produce the MOF. Details on sample preparation are also included in this chapter,

including the microrod alignment for the resin samples and the capillary cell preparation for the liquid suspension samples.

Chapter 4 displays the results from both the polarisation of absorption and polarisation of emission experiments. Results include the fluorescence intensity measurements from suspension samples and three differently-aligned resin samples.

The final chapter, 5, discusses the conclusions drawn from the research including potential future work and applications.

1.2   Brief History of MOFs

MOFs were first introduced over two decades ago in the early 1990s, with the term MOF being coined in 1995, as an exceptionally stable and highly porous class of crystalline hybrid materials, composed of bonds between organic ligands and metal ions, with extraordinary large surface areas [5]. They can be assembled to produce 1, 2 or 3-Dimenional structures and, with the ability to alter the metal and/or ligand used in synthesis of MOFs, over 20,000 variations have now been synthesised and characterised [6]. Each variation has the potential to have its own unique properties and applications. MOFs currently have applications in areas such as gas separation, storage and sensing, for removing unwanted or harmful molecules from a mix, catalysis and electrochemical energy storage for use as electrodes, with more application potential continually being discovered [7].

2 Literature Review

2.1 General MOF Structure and Properties

MOFs are hybrid crystalline structures generally consisting of positively charged metal ions (nodes) linked to organic ligands by means of reticular synthesis - the process of creating a molecule with such components by forming strong bonds throughout a crystal assembled from rigid secondary building units and ordered structures [8-10]. This coordination network can extend in up to three dimensions, with infinite repeating patterns. As a result of these combinations of building blocks, there is the potential for an infinite number of variations of MOFs, each with different structures, building units and applications. In the short history that MOFs currently have it is amazing to think that tens of thousands have already been reported [11]. The shape of the molecule formed as a result of a MOFs structure, with an almost hollow structure as seen in Figure 2.1, gives rise to two very important properties – very high porosity and very large surface areas [12].
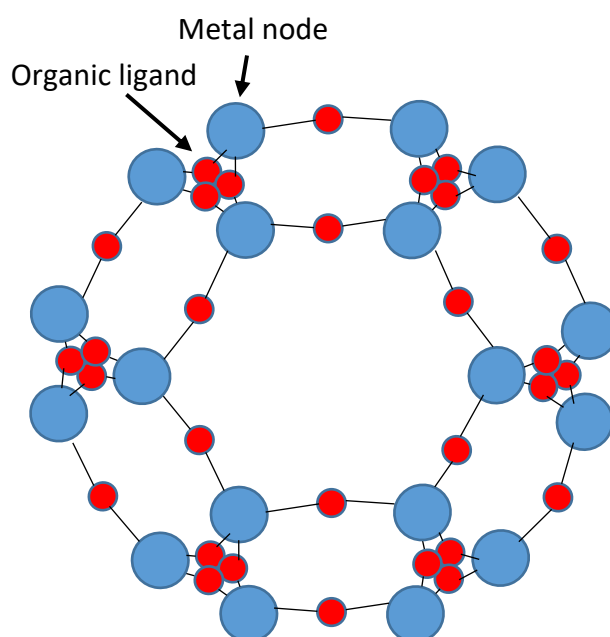
Figure 2.1: Illustration of a generic MOF structure with metal ions (blue) and organic ligands (red) and demonstrating their cage-like structure.

Their high porosity gives rise to their well-known superior ability to capture and release molecules and the extraordinary surface area, currently reported as up to 7000 sqm/gram, make them very useful in applications such as gas sensing and separation, outlined further in this chapter, and in many cases improve upon similar properties possessed by zeolites – which have current uses in carbon dioxide separation [13,14].

2.2 MOF Applications

There are a number of MOFs that are already being synthesised today with their unique properties being exploited for a variety of applications. This chapter outlines some of those MOFs and how they may prove to be useful in the near future. Such applications display how every one of the many variations of MOFs have the potential to be utilised for specific needs. The ideal MOF for each application can be synthesised by, for example, altering the metal node to find MOFs with the ideal properties for an application such as a larger surface area or larger pore sizes.

2.2.1 Gas Capture

In gas capture and separation, MOFs with a very large surface area prove useful to be utilised to remove certain molecules from a gas mixture, particularly in an aqueous solution. The large surface area and pore sizes demonstrated by these materials offer a lot of space for guest molecules to enter and be trapped. The M-MOF-74 displays these properties, where 'M' represents a transition metal ion – typically Zn, Ni, Co or Mg. The M-MOF-74 consists of $M_2O_2(CO_2)_2$ chains linked by the

2,5-dioxidoterephthalate (DOT) ligand and the resulting molecule, shown in Figure

2.2, exhibits ultrahigh pore sizes [15].

2,5-dioxidoterephthalate (DOT)

+

$M_2O_2(CO_2)_2$
1D chain
(M: Zn, Co, Ni, Mg)
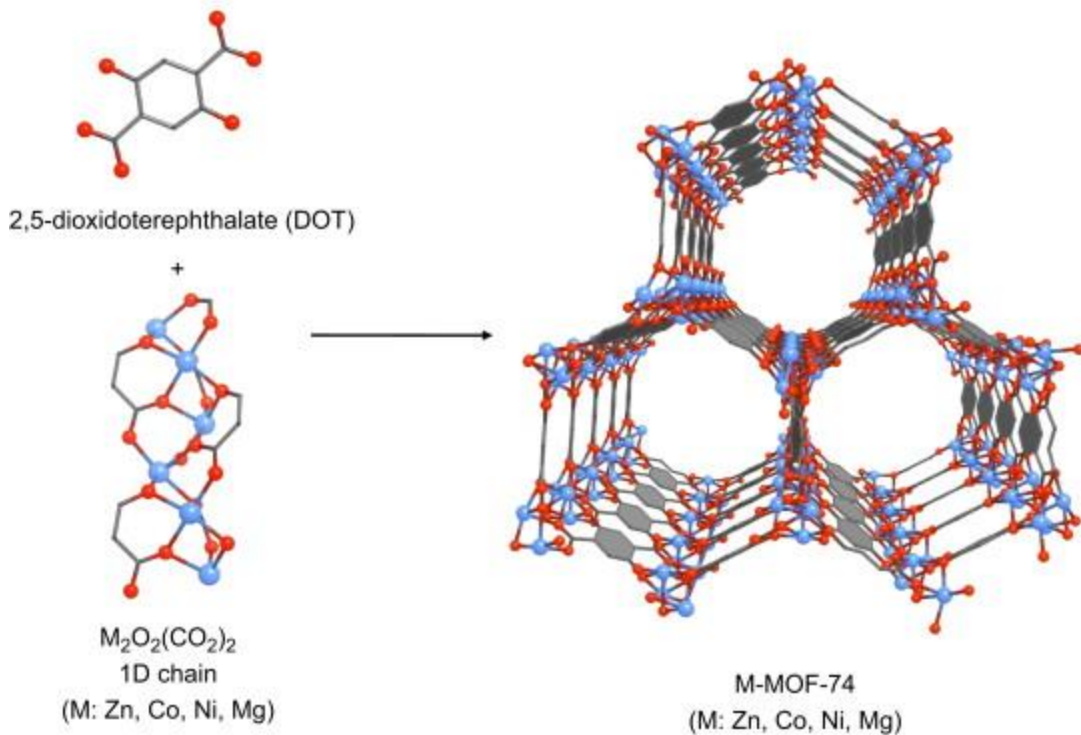
M-MOF-74
(M: Zn, Co, Ni, Mg)

Figure 2.2: M-MOF-74 synthesis, where 'M' represents a metal ion. [15]

The magnesium-based MOF-74 has been shown to be particularly effective at

capturing CO_2 gas molecules. For example, it is well known that global warming is

becoming an increasing cause for concern due to the amounts of CO_2 being released

into the atmosphere. There are a number of potential techniques that, by exploiting

the large surface area and pore sizes of Mg-MOF-74, can be used to remove the CO_2

and other harmful greenhouse gases from the atmosphere or perhaps before it even

reaches there in order to reduce the damage the gas inflicts on our planet [16].
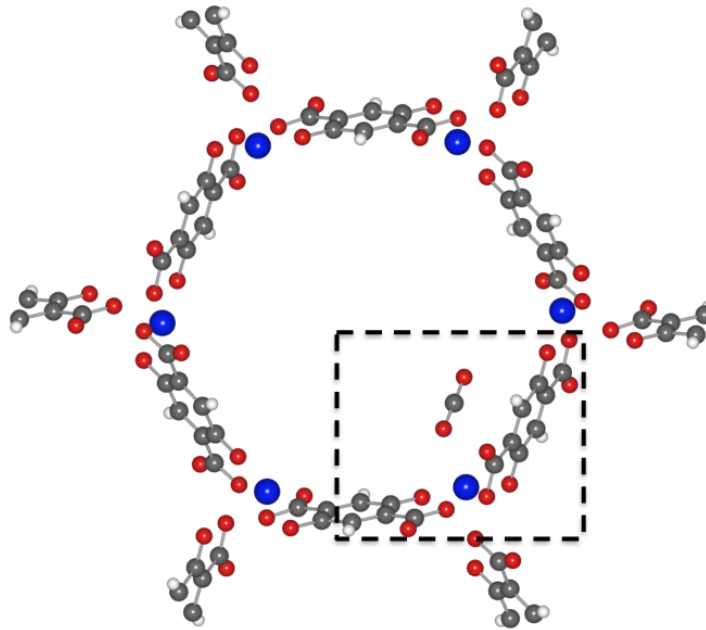
Figure 2.3: M-MOF-74 structure with a molecule of CO_2 adsorbed at one of its OMSs (open metal sites). [17]

This MOF possesses such an ability due to its high density of open metal sites (OMSs). Figure 2.3 demonstrates how the Mg-MOF-74 is able to trap a molecule of CO_2 by strongly binding it with an OMS. However, the OMSs are much more preferably occupied by H_2O molecules and so they are much more effective at tackling CO_2 removal under dry conditions [16, 17]. This could prove to be a drawback for the use of this MOF for CO_2 capture if these favourable conditions are not able to be achieved. Therefore, using this MOF for gas capture of CO_2 in higher altitudes of the atmosphere could prove very effective but at lower altitudes, where the atmosphere contains water vapor, it would be much less effective.

2.2.2 Gas Sensing

Other magnesium-based MOFs, such as the M-MOF-I and M-MOF-II, can be used similarly for gas sensing by adsorption of gases onto the surface of the sensor [18]. Such MOFs make for good sensors primarily due to their higher surface areas and thermal stability compared with other MOFs. Both the M-MOF-I and M-MOF-II consist of infinite, rod-shaped building blocks, $M_3[(-O)_3(-CO_2)_3]$, where M in this case is Mg for comparison with the Mg-MOF-74 [18]. Joining this metal cluster with either the linkers TDA^{4-} or ODA^{4-} results in the honeycomb-shaped structures of Mg-MOF-I and Mg-MOF-II respectively, as in Figure 2.4 [18].
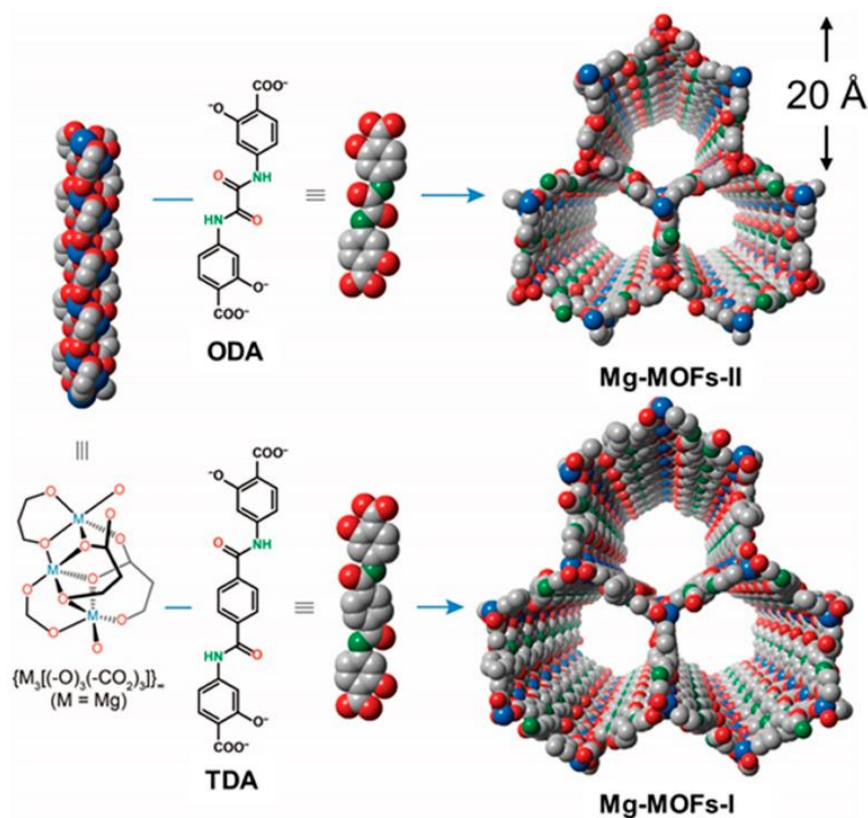
Figure 2.4: Structures of the Mg-MOF-I and Mg-MOF-II, displaying their honeycomb shape and large pore sizes. [18]

This structure results in more adsorption sites, so more area for target gases, and a more effective sensor response compared to regular Electrochemical or Metal Oxide Semiconductor sensors.

a)

b)
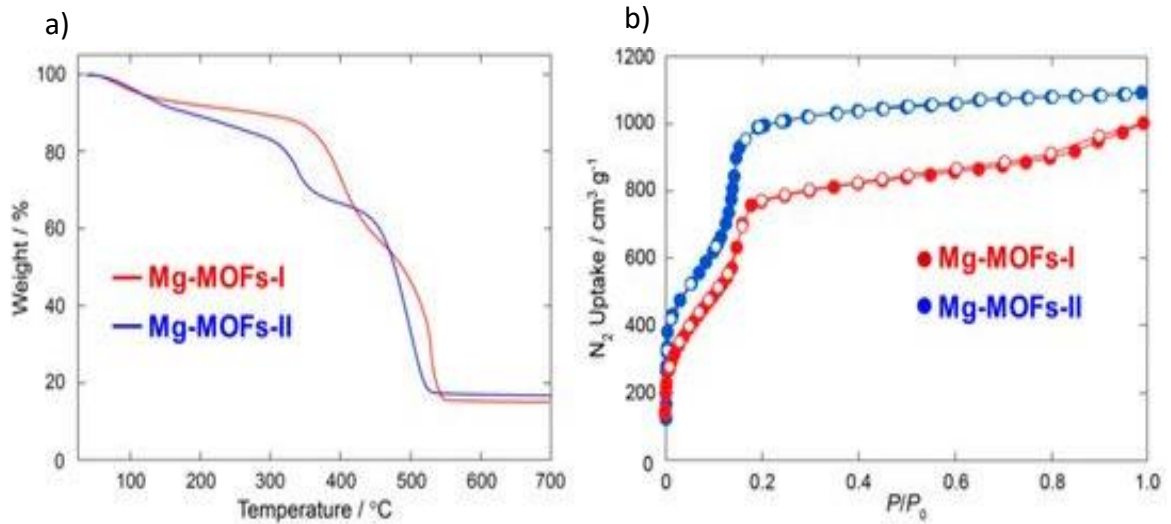
Figure 2.5: a) TGA (thermogravimetric analysis) curves of Mg-MOF-I and Mg-MOF-II and b) N_2 intake for examination of porosity under pressure. [18]

Although still magnesium-based, the Mg-MOF-I and II have been shown to be much more thermally stable than Mg-MOF-74. The thermogravimetric analysis (TGA) curve in Figure 2.5a demonstrates how the MOF is able to operate stably up to temperatures of around 300^0C. The curve in Figure 2.5b shows how effective the MOFs are at up taking N_2 at a set temperature (77K) with varying pressure.

2.2.3   Energy Storage

Altogether differently built MOFs, such as the iron-based MIL-53, have proved to be particularly useful for applications in electrochemical energy storage in Lithium-Ion Batteries (LIBs) and capacitors [19].
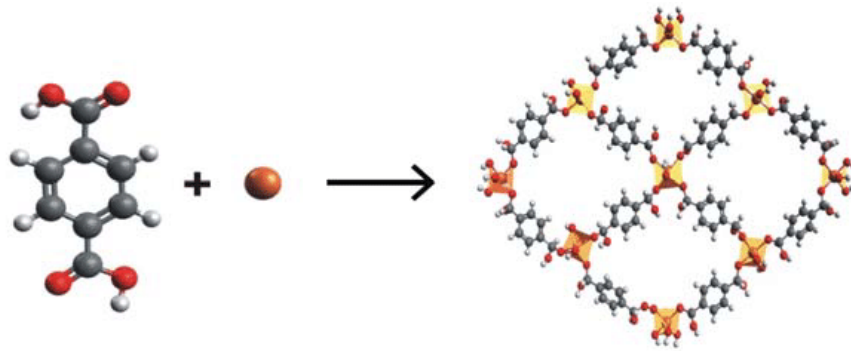
Figure 2.6: Structure of MIL-53 (Fe). [20]

The MIL-53 (Fe) MOF, shown in Figure 2.6, consists of 1,4-benxendicarboxylate ligands linked to infinite chains of trans-corner-shared octahedral units – in this case FeO_6 as defined in the notation 'MIL-53 (Fe)' [20].

It has been shown that both iron and lithium ions were able to be inserted between the layers of the crystal lattice with no structural deformation or alteration for use. Such experiments make MIL-53 an outstanding potential material for use as an electrode due to its high electrical conductivity and modifiable pore size. MOFs with this ability could prove of paramount importance to combat the energy crisis [19]. This is due to their high efficiency and energy density, environmentally friendly properties and that the materials required to produce them are abundant in nature, providing low-cost solutions [19]. For example, such methods have been attempted for development of Sodium-Ion Batteries (SIBs), however sodium ions are much larger and heavier than lithium ions leading to unsuccessful insertion [19].
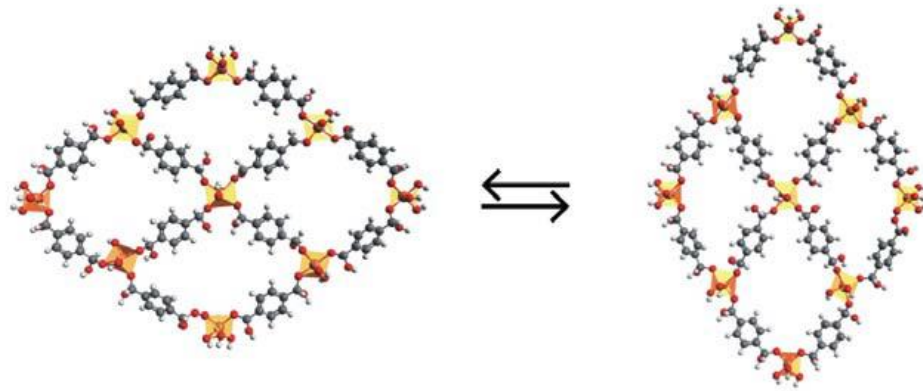
Figure 2.7: Display of MIL-53 (Fe) reversible ability to open and close its pores. [20]

An unusual property of MIL-53 (Fe) is that it does not have a particularly large surface area in comparison with most other MOFs. On the other hand, it possesses a unique feature with a very flexible structure which allows it to open and close its pores, as in Figure 2.7. This property provides applications in gas capture and adsorption; however, this MOF is very expensive to produce, are complex to synthesise and are toxic in nature [20].

2.2.4   Catalysis

The permanent high-porosity nature of MOFs can be taken advantage of for applications in catalysis. Experiments previously performed on the copper-based Cu-MOF-74 found it to be of very high stability and catalytic activity at a range of temperatures, seen in Figure 2.8 [21]. This is another variation of the M-MOF-74 demonstrated in section 2.2.1, where 'M' is copper. This MOF possesses a very high OMS density, which is directed into the open pore of the MOF [22].
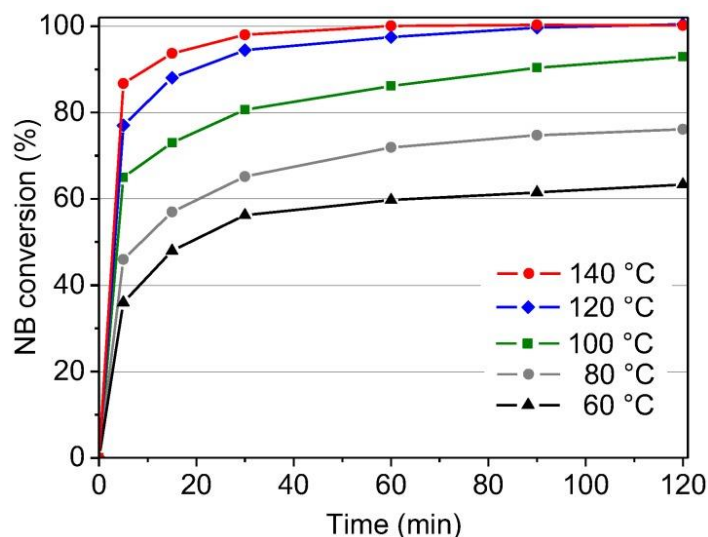
Figure 2.8: 4-nitrobenzaldehyde (NB) conversion catalysed by Cu-MOF-74 at varying temperatures. [21]

Figure 2.8 demonstrates how the Cu-MOF-74 is extremely effective as a catalyst, in this case to NB (4-nitrobenzaldehyde) conversion, at a range of temperatures. This conversion takes place by means of a cross-coupling reaction between NB and phenol to form an ether [21]. This is particularly significant as the ether produced as a result of this conversion (4-formyldiphenyl ether (FDE)) can be used to synthesise natural products for pharmacology, for example [21]. At higher temperatures of 120°C and 140°C Cu-MOF-74 proves to be highly active, with NB conversion at 80-90% in under five minutes [23].
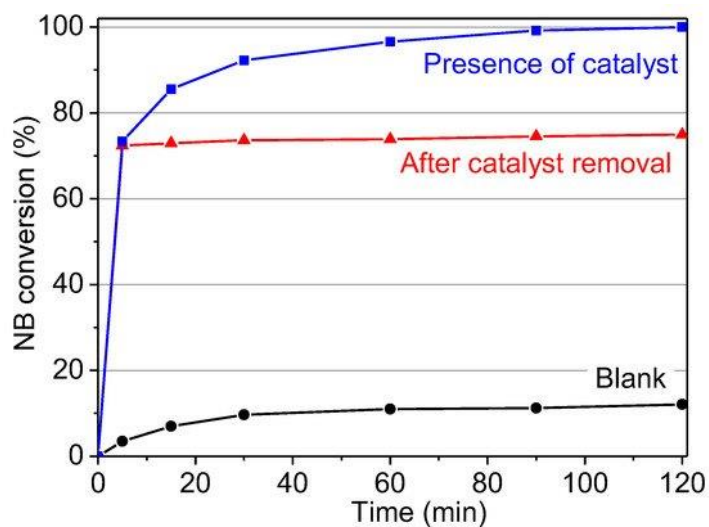
Figure 2.9: Conversion of NB with (blue) and without (black) Cu-MOF-74 catalyst present [21].

Figure 2.9 demonstrates the important role that the MOF plays as a catalyst in this reaction. Without it, labelled 'Blank', the NB conversion barely rises above 10%. The blue line represents the NB conversion with the catalyst present, and the red line with the catalyst present and removed after 5 minutes – both of which demonstrate significantly higher NB conversion [21].
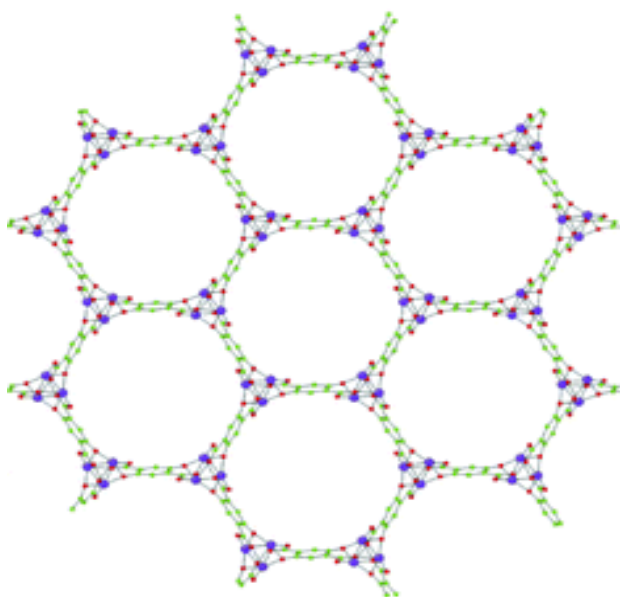
Figure 2.10: Cu-MOF-74 honeycomb structure. [22]

Cu-MOF-74 consists of $Cu_2O_2(CO_2)_2$ chains linked by the 2,5-dioxidoterephthalate ligand, resulting in a honeycomb structure as shown in Figure 2.10.
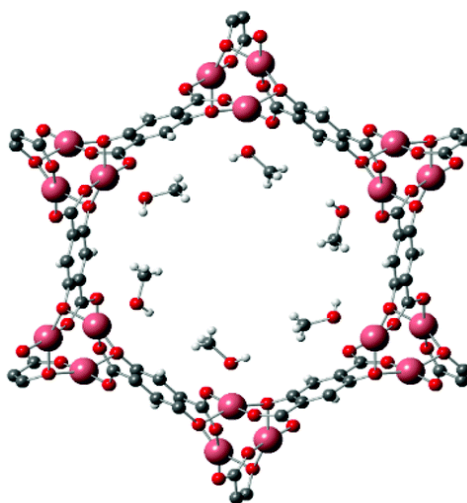
Figure 2.11: Pore structure of Cu-MOF-74 with molecules of MeOH inside the channel. [23]

Figure 2.11 demonstrates how Cu-MOF-74 is utilised for catalysis, with molecules in the channel near the Cu OMSs [23]. This copper-based MOF is favourable for catalytic reactions over other copper-based MOFs due to its very large pore sizes, resulting in easier diffusion within its structure as well as having a much higher activity than other copper catalysts previously tested due to its unsaturated copper sites [21, 23, 24]. The Cu-MOF-74 possesses the ability to be reused multiple times in succession as a catalyst with very little alteration in stability between uses at a variety of temperatures from 60-140°C.

2.3 NU-1000 MOF

This section outlines the key features of the MOF used in this study.

2.3.1 Structure and Applications

NU-1000 is zirconium-based (Zr_6) and comprises of eight $Zr_6(\mu_3$-$OH)_4(\mu_3$-$O)_4(OH)_4(OH_2)_4$ metal nodes linked by the organic tetratopic pyrene-based ligand ($TBAP_y^{4-}$, 1,3,6,8-tetrakis(p-benzoate)) pyrene [25]. It is the strength of the bonds between the zirconium nodes and organic ligands that provides this particular MOF, as well as some other Zr-based MOFs, with such high thermal and chemical stability, leading to them being superior supports for catalysts and gas separation [25]. NU-1000 has previously been used to separate and adsorb furanics – a toxic, heterocyclic organic compound (C_4H_4O) – from sugars, allowing for much greater efficiency of production of biomass products [26].
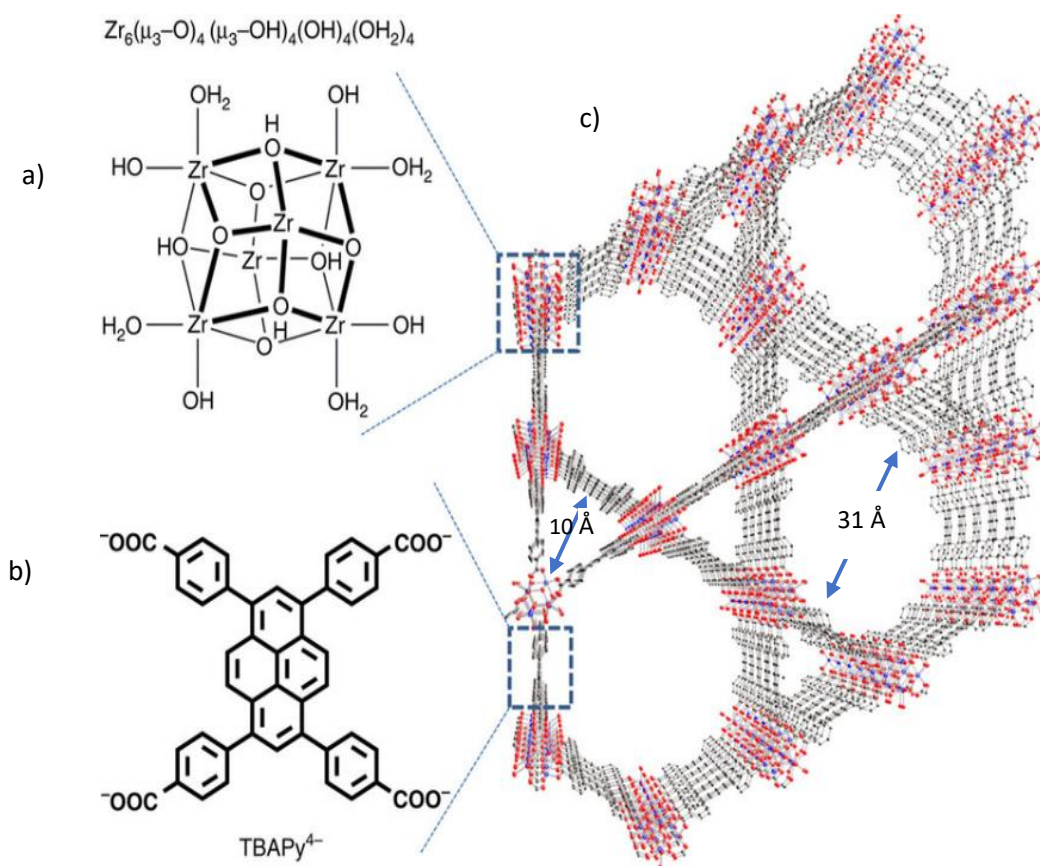
Figure 2.12: Illustration of the a) metal nodes and b) pyrene ligands present in the c) NU-1000 MOF crystal structure. Pore sizes are indicated in Figure 12c. [27]

Shown in Figure 2.12, due to its honeycomb-like shape, NU-1000 contains pores of two different sizes. Its smaller pores have a diameter of 10 Å while the larger pores have a diameter of over three times that, at 31 Å [28]. This large pore size is what makes it extremely efficient as a catalyst, allowing for very rapid diffusion [26-28], as discussed above in section 2.2.4.

The reasoning behind choosing this particular MOF over the thousands of other varieties is primarily due to their rod-shaped microcrystals, shown in Figure 2.13, chemical stability and many potential applications. The anisotropic properties associated with such a shape will provide us with invaluable information on their magnetic and electric functionalisation. The rod shape crystals experience a torque, as explained in section 2.6, which will make it much easier to determine if they are successfully aligned – particularly visibly under a microscope. The very strong bonds between the acid-hard base Zr^{IV} atoms and carboxylate oxygens provide outstanding chemical and thermal stability, with uses up to 500°C and between 1-11pH [29].
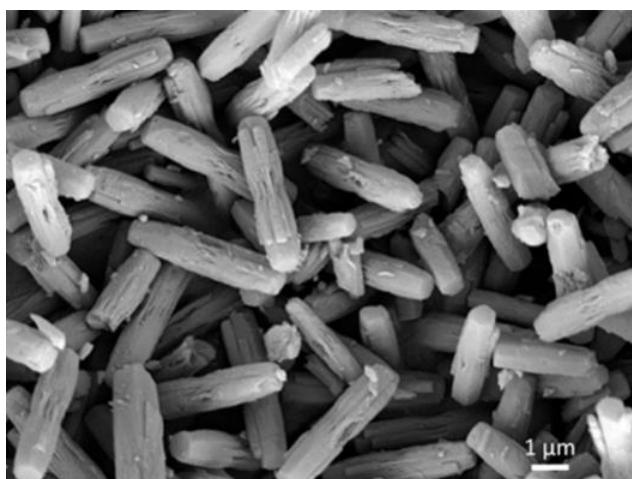
Figure 2.13: SEM image of NU-1000 microrods.

2.4   Emission Spectra

We can look at the separate emission spectra of the TBAP$_y^4$ pyrene ligand and compare it with that of NU-1000. This will determine how the ligand is modified once inside the NU-1000 structure.

2.4.1   TBAPy^{4-} Pyrene Ligand Emission Spectrum

Previous literature demonstrated the emission spectrum of the pyrene ligand with a similar excitation wavelength to ours, 395nm, depicted in Figure 2.14.
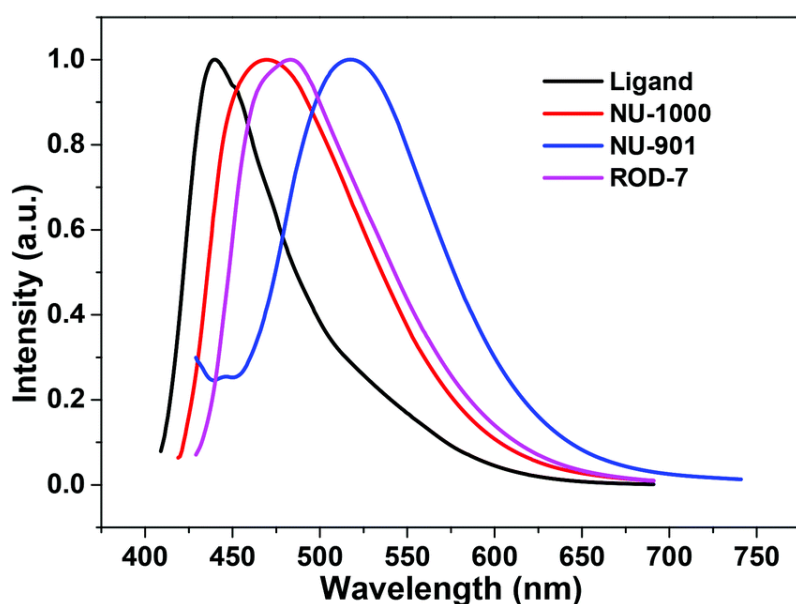
Figure 2.14: NU-1000 (red) and ligand (black) emission spectra with excitation wavelength 395nm. [30]

The emission peaks of TBAPy^{4-} and NU-1000 appear at 440nm and 465nm respectively with a 395nm excitation wavelength – only a 25nm emission red shift. This very small shift is due to the Zr^{4+} ions in the MOF possessing closed shells making it very difficult to excite them, leaving the ligand transition undisturbed [30].

2.4.2 NU-1000 Emission and Absorption Spectra

The reason for the choice of laser, used in this thesis, of wavelength 405nm is to maximise the absorption and emission properties of the NU-1000 MOF. Figure 2.15, taken from previous work on properties in zinc-based MOFs, displays the absorption spectrum for a solid NU-1000 sample (blue) [31]. It indicates that 405nm is a suitable steady-state electronic absorption wavelength.
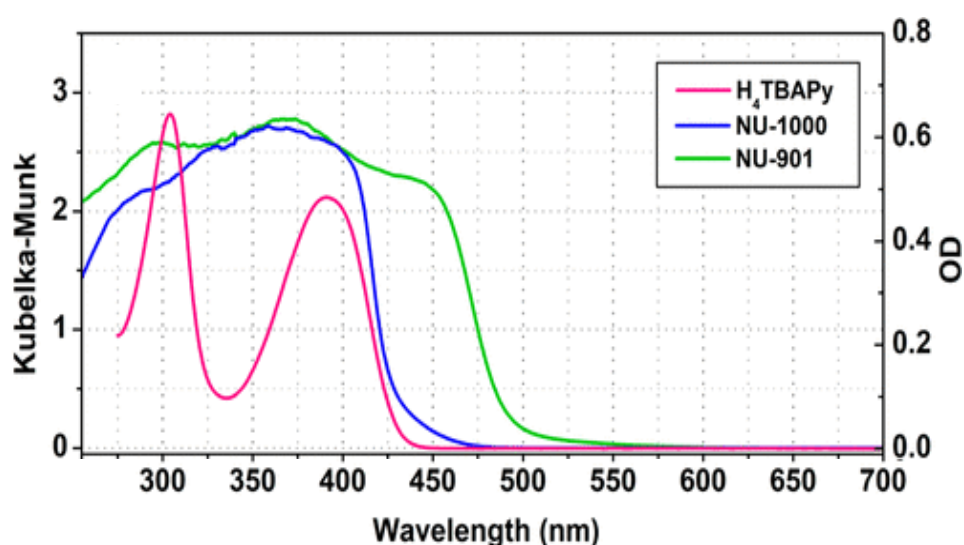
Figure 2.15: Electronic absorption spectra, including diffuse reflectance spectra of solid NU-1000 (blue). [31]

Previous work, as in Figure 2.16a and 2.16b, also exhibits the excitation-emission mapping spectra for NU-1000 in different solvents - 3-MePent and MeCN [32]. They indicate that the more intense emission peaks both appear just below 475nm with an excitation wavelength of 395nm, despite the difference in used solvents. This data suggests that the emission transition energies are relatively unaffected by solvent polarity. However, the double intense emission peak in Figure 2.16b, with excitation wavelengths of 395 and 425nm suggests that the emission may be affected by solvent polarity and is more effective with polar solvents. It is also suggested that it

becomes particularly effective in polar solvents with a high acceptor number (AN).

The AN of a solvent is defined as the electrophilic properties of that solvent – its

ability to accept or attract electrons – based on the ^{31}P-NMR chemical shift of

$C_6H_{15}OP$ in the solvent [32]. The solvent we used, bromobenzene (BrPh), is a non-polar

solvent and so should not have such an effect on results.
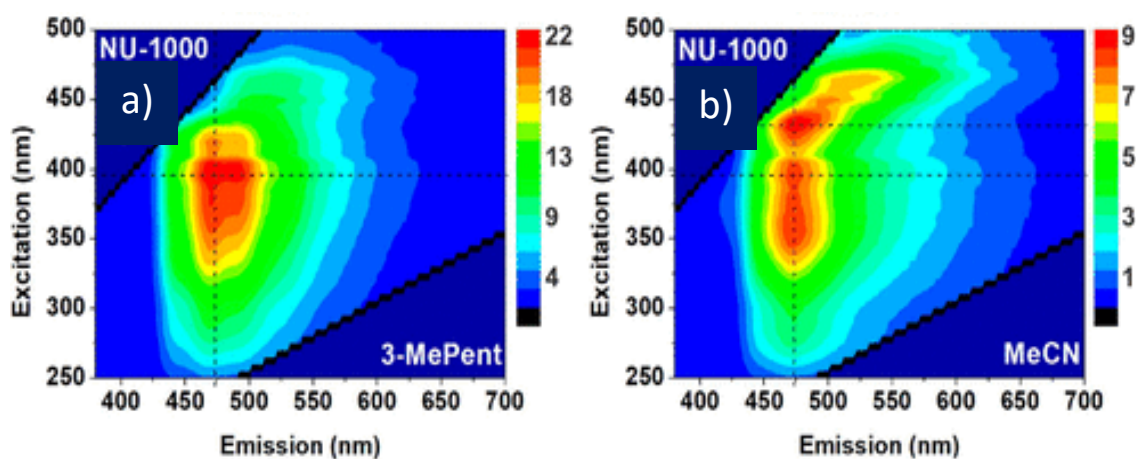
Figure 2.16: Excitation-emission spectra for NU-1000 suspended in a) 3-MePent and b) MeCN. [32]

2.5   Excitation and Fluorescence

This section discusses two important concepts, excitation and fluorescence, which are utilised during this study.

2.5.1   Excitation

When an electron, usually in ground state, absorbs a discrete amount of energy it becomes raised to a higher, unstable state – this is called excitation. The energy absorbed is often in the form of a photon, where the amount of energy, E, a photon possesses is calculated by *(1)*, where h is Planck's constant (6.64×10^{-34} Js) and f is the frequency of the light.

$$E = hf \tag{1}$$

The difference in energy between the ground (E_1) and excited states (E_2) is equal to that of the absorbed photon energy. In order for the electron to transition back to a lower energy level or back to ground state, it must emit a photon with an energy equal to the difference between the two states (E_2-E_1), shown in *(2)*. This process is called de-excitation.

$$\Delta E = E_2 - E_1 \tag{2}$$

In this instance, no energy is lost and so the emitted photon has the same wavelength as the absorbed photon.

2.5.2   Fluorescence

In the case that a photon, or photons, not only interact with a single electron but with an atom, molecule or sample, the energies of the absorbed and emitted photon can differ.
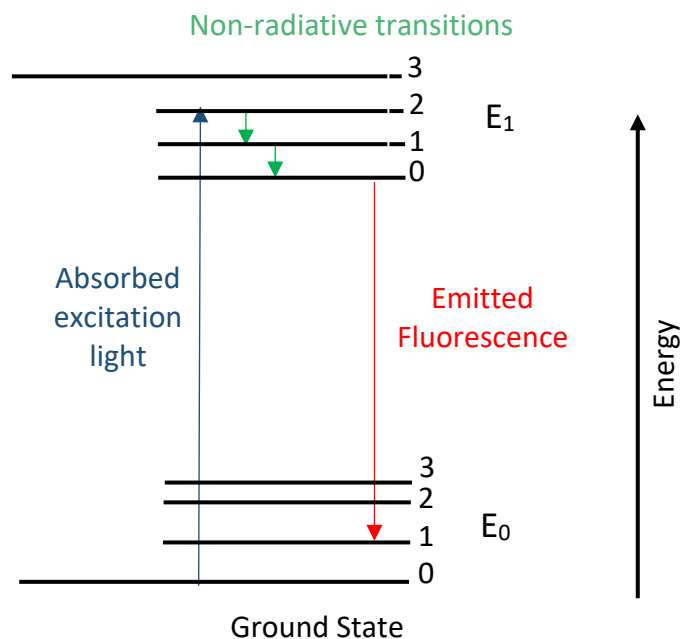
Figure 2.17: Basic energy level diagram for fluorescence.

The energy level diagram in Figure 2.17 demonstrates how a photon may interact with a molecule. A photon is absorbed, raising the electron to a higher energy level. This process has a timescale of around 10^{-15} seconds. During the time spent in the higher energy levels, usually lasting between 10^{-12} and 10^{-10} seconds, the photon can interact with the sample and undergo non-radiative transitions, in the form of vibrational relaxation. A non-radiative transition is a transition that occurs without absorption or emission of photons occurring. The average time the molecule remains in an excited state is known as the fluorescence lifetime. A photon is then emitted. Having lost energy due to the non-radiative transitions, the emitted photon has a lower energy than that of the absorbed photon, thus has a longer wavelength as according to the photon energy equation *(1)*. This emission is called fluorescence – takes between 10^{-10} and 10^{-7} seconds.
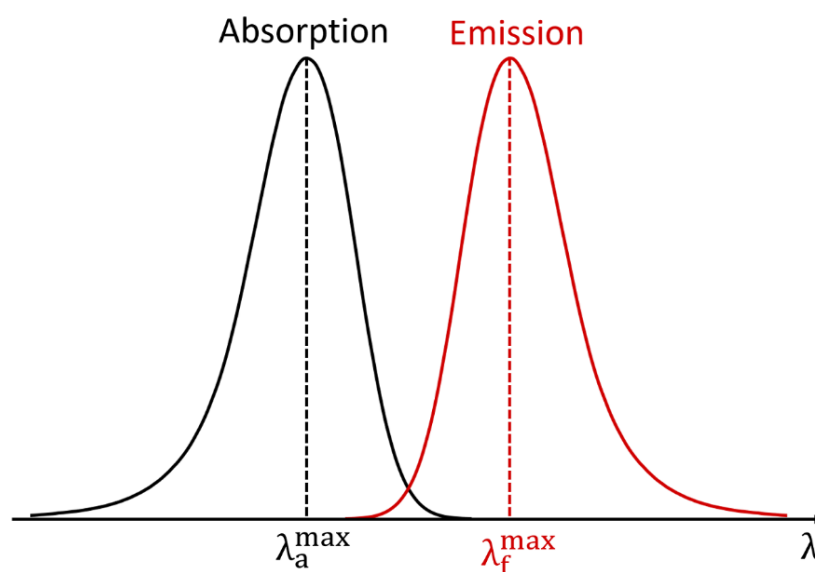
Figure 2.18: How Stokes Shift is quantified. [33]

The resulting difference between the wavelength of the maximum absorption and fluorescence emission is known as Stokes Shift, shown in Figure 2.18. Stokes Shift varies depending on the sample's fluorophore and environment (solvent), for example, less polar solvents have a much smaller Stokes Shift than more polar solvents, which have a much larger Stokes Shift.

Stokes Shift can be very well represented in the form of a Perrin-Jablonski diagram – a more advanced energy level diagram than in Figure 2.17 - which illustrates the possible radiative and non-radiative transitions that can occur, shown in Figure 2.19. Transitions can occur within singlet states (system with no unpaired electrons and total spin angular momentum of zero) or triplet states (system with two unpaired electrons and total spin angular momentum of one). Possible transitions are singlet-singlet transitions, singlet-triplet transitions and triplet-singlet transitions.
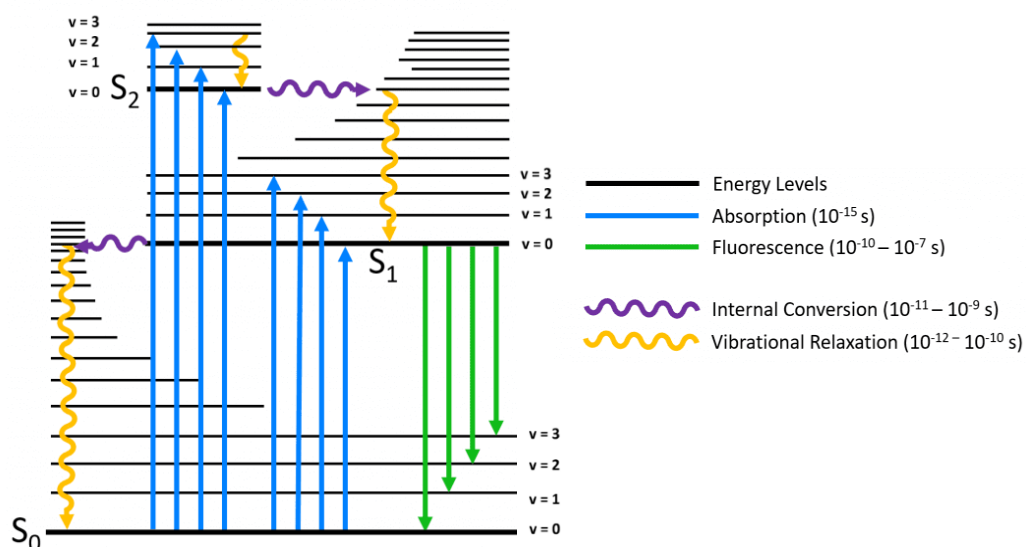
Figure 2.19: Perrin-Jablonski diagram illustrating all possible absorption and fluorescent transitions between singlet states. [34]

For regular fluorescence to occur, we are only concerned with transitions within the singlet states, S_n, therefore no 'intersystem crossing' takes place. S_n represents the electronic energy levels and v_n represents the vibrational states. In order for Stokes Shift to occur, the absorbed photon must be raised to a vibrational state higher than the vibrational state that the fluorescence occurs from. For example, if the absorption transition was S_0, v=0 to S_1, v=0, and the fluorescence transition was S_1, v=0 to S_0, v=0, there would be no Stokes Shift. A Stokes Shift transition would therefore be, for example, an absorption transition from S_0, v=0 to S_1, v=2 and fluorescence transition from S_1, v=0 to S_0, v=3.

2.5.2.2 Franck-Condon principle and Born-Oppenheimer approximation

The intensity of these vibrational transitions, as well as the probability of a transition happening to and from a particular vibrational state occurring, is determined using the Franck-Condon principle. This, along with the Born-Oppenheimer approximation, state that because nuclei are so much more massive than electrons and so move

much slower in comparison to the very fast electronic transition, the nuclei can be considered fixed during the transition and thus the motion of nuclei and electrons in a molecule can be considered separately.
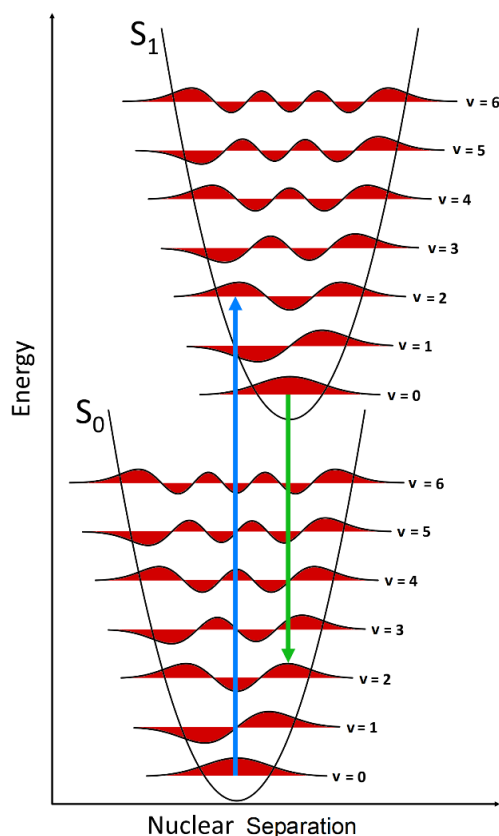
Figure 2.20: Energy diagram displaying the Franck-Condon principle. [33]

The energy diagram in Figure 2.20 illustrates the Franck-Condon principle, at room temperature for a diatomic molecule, with the black quadratic curves representing the potential wells of the nuclear separation and the red curves representing the wavefunctions of the vibrational levels. This transition probability is given by Fermi's Golden Rule. The Maxwell-Boltzmann distribution represents the probability that a system will be in a certain state. In this case, the probability that an electron will be in a certain vibrational state. As a result, shown in Figure 2.20, most of the absorption occurs from S_0, v=0. The strongest transition, and maximum wavelength of the

absorption spectrum, is represented likewise and occurs where there is the greatest overlap of wavefunction amplitudes between S_0, v=0 and all vibrational S_1 states, in this case S_1, v=2. The absorption transition will always be to S_1, v>0 due to the separation between the nuclei.

Fluorescence always occurs from S_1, v=0 due to the rapid vibrational energy loss. Again, the strongest fluorescence transition occurs where there is the greatest overlap of wavefunction amplitudes between S_1, v=0 and all vibrational S_0 states, in this case S_0, v=2. As a result, the maximum intensity of the fluorescence spectrum will always be a longer wavelength than that of the absorption spectrum. This difference in wavelength is where the previously mentioned Stokes Shift arises.

2.5.2.3 *Photobleaching*

Any process which reduces the fluorescence ability or intensity of a sample is referred to as fluorescence quenching [35]. A factor that can affect a molecule's ability to fluorescence and contribute to fluorescence quenching is photobleaching, which is the potentially irreversible damage of the fluorophore, leaving the molecule unable to fluoresce either partially or entirely. The main reason photobleaching occurs is due to the excitation intensity being too high, altering the structure of the fluorophore [36].

2.6   Dipoles

There are two types of dipoles in electromagnetism; magnetic dipoles and electric dipoles. For this thesis we will only be concerned with electric dipoles and how they arise within molecules.

2.6.1 Electric Dipole Moment

An electric dipole occurs due to the separation between the positive and negative charges of a system. As a result of this separation, they possess a dipole moment, p, which determines a system's polarity. Dipole moments are a vector quantity which points from negative to positive.

$$\overline{p} = q\overline{d} \qquad\qquad (3)$$

The magnitude of an electric dipole moment can be calculated using *(3)*, where q is the magnitude of the charge and d is the separation distance.

Molecules can exhibit an electric dipole moment due to the random distribution of positive and negative charges from each atom [37]. In a molecule, electronegativity is used to measure the tendency of an atom to attract a bonding pair of electrons. For the most basic molecules, diatomic molecules, the electronegativity of each atom affects the attraction of the shared electron pair. The atom which is more electronegative tends to attract the electron pair more than the lesser electronegative atom, producing the separation required to create a dipole.

Electronegativity is often measured using the Pauling scale, ranging from 0.7 (least) to 4.0 (most) and depends on three factors; the distance between the protons in the nucleus and the electrons in the valence shell, an atom's nuclear charge, and the electron shielding effect. The force between positive and negative charges depends on the inverse-square law – the greater the distance, the lower the force. Nuclear charge determines that the greater the number of protons in the nucleus, the greater attraction there is on electrons. However, the larger the number of electrons, the

greater the effect of shielding – electrons in inner shells shield the effect the protons have on the valence electrons. As a result, the most electronegative atom is fluorine while francium is the least.

In a diatomic molecule consisting of two different atoms each with different electronegativity, HCl for example, the more electronegative chlorine will attract the electrons more than the hydrogen, shown in Figure 2.21 - chlorine has an electronegativity of 3.0, while hydrogen has only 2.1.

$$\delta+ \quad\quad \overset{\text{x}}{\underset{\text{x}}{H \rule{3cm}{0.4pt} Cl}} \quad \delta-$$
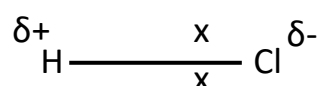
Figure 2.21: Electronegativity displayed in HCl, with electrons 'x' more strongly attracted to the chlorine atom.

As a result, there is an increase in electron density towards the chlorine end of the bond and reduction at the hydrogen end, producing slightly more negative and positive ends respectively, represented by the δ+ and δ– respectively.

In a diatomic molecule where each atom is equal in electronegativity – for example if they are identical hydrogen atoms – then the attraction to the electron pair from each atom is equal. Therefore, the electron pair are, on average, equidistance between the two atoms, as in Figure 2.22, since each atom has an electronegativity of 2.1.

$$\overset{\text{x}}{\underset{\text{x}}{H \rule{3cm}{0.4pt} H}}$$
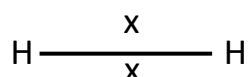
Figure 2.22: Electronegativity displayed in H_2, with electrons 'x' equally attracted to each hydrogen atom.

There are three types of dipoles that can occur for molecules as a result of electronegativity – permanent, instantaneous and induced dipoles. Permanent dipoles occur when the two bonded atoms have significantly different electronegativities, as with hydrogen and chlorine in Figure 2.21, creating a polar molecule. Instantaneous dipoles occur when the bonded atoms have the same, or similar, electronegativities due to the movement of electrons, so only occur for an instant, as in Figure 2.22, creating a non-polar molecule. Induced dipoles occur due to the interaction between polar and non-polar molecules, whereby the polar molecule repels the electrons in the non-polar molecule, inducing a dipole, as if a molecule of HCl were to be in close proximity to a molecule of H_2, the HCl would induce a dipole in the previously non-polar H_2 molecule.

As a result of the dipoles created by the non-uniform distribution of electrons, molecules can experience a torque when within an external electric field in order to try and align the dipole moment with the electric field.

r_a = semi-major axis

r_b = semi-minor axis
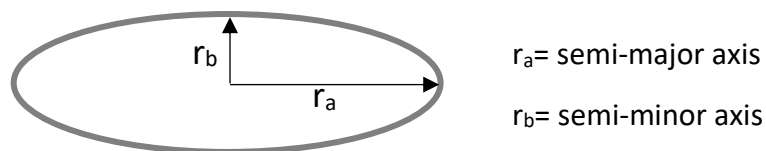
Figure 2.23: Axes for an ellipse.

If we consider the molecules as elliptical microrods, for the purposes of this thesis, one end of the polar molecule will be slightly positively charged, the other slightly negatively charged – a dipole. The axes of this microrod, shown in Figure 2.23, can be represented as an aspect ratio z, which is the ratio of the semi-major axis to the semi-minor axis, $z = r_a/r_b$ - the major and minor axes are given by $2r_a$ and $2r_b$ respectively.
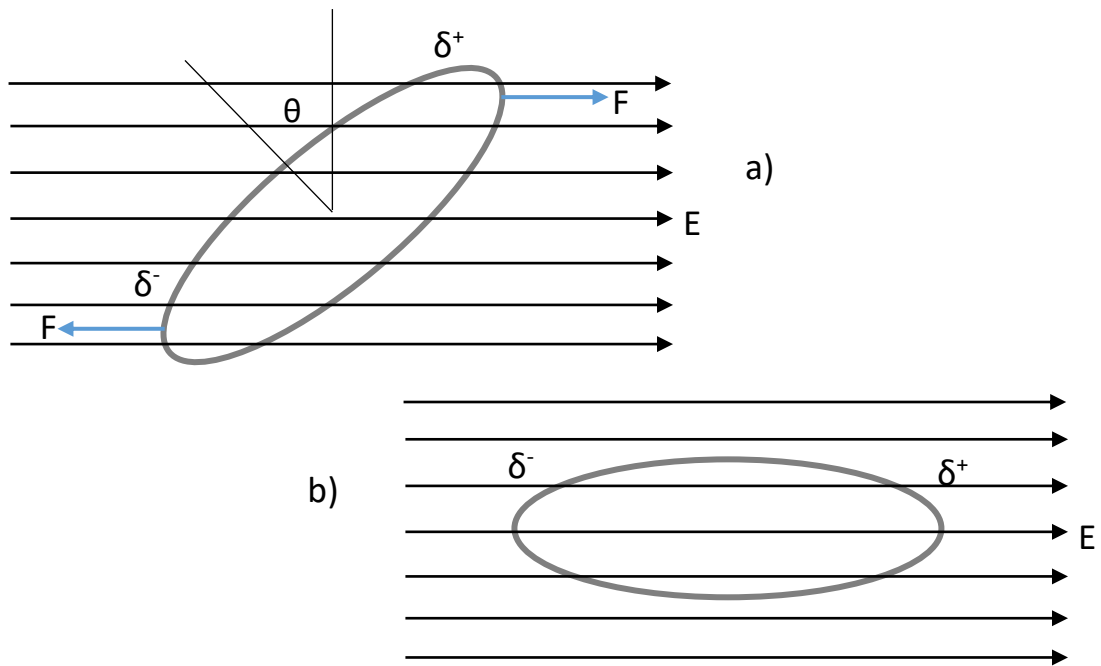
Figure 2.24: Schematic of the effect an applied, uniform electric field has on an electric dipole in terms of a) the torque applied and b) an aligned dipole.

Applying an electric field produces a force F=qE to the positive charge side and a force F=-qE to the negatively charged side of the microrod.

$$\tau = |p|\ |E|\sin\theta \qquad (4)$$

This produces a torque, with magnitude given by *(4)*, where Ɵ is the microrod elevation angle from parallel to the electric field, resulting in the microrods major axis aligning parallel to the direction of the external electric field, demonstrated in Figure 2.24b.

2.6.2 Transition Dipole Moment

When a molecule undergoes a transition between an initial and final state, as when it absorbs a photon and is raised from ground state to a higher energy level, a transition dipole moment can occur. A transition dipole moment can only occur when there is a difference in the charge distribution between two orbitals that the

transition is occurring – otherwise there is no dipole produced. For example, if the molecule were to transition from a lower s orbital (1s) to a higher s orbital (2s), there is no alteration in the charge distribution since the orbitals are the same shape and so there is no change in the dipole. If, however, there was a transition from a lower s orbital (1s) to a higher p orbital (2p), for example, then there is a change in the distribution of the charge since the orbitals have different shapes. This means that there is a change in the dipole moment, resulting in a transition dipole moment.

$$\mu_e = \int \int \int \Psi_f \, \mu \, \Psi_i \, dxdydz \ ^{(38)} \qquad\qquad (5)$$

Equation *(5)* can be used to determine the height of absorption peaks for a photon and relates to the integral of the transition dipole moment. This consists of the product of the wavefunctions of the initial and final states, Ψ_i and Ψ_f respectively, and dipole moment operator, μ, all integrated over space [38].

By using this equation, without the need for inserting numbers, it is evident that for transitions between same-shaped orbitals (such as 1s to 2s as mentioned above), the dipole moment integral would be zero due to there being no change in distribution of the charge during the transition. As a result, this is a forbidden transition. Similarly, for transitions between differently-shaped orbitals (such as 1s to 2p as mentioned above), the dipole moment integral is non-zero due to there being a difference in charge distribution, meaning there is a reorientation in the dipole moment. This is an allowed transition, resulting in a peak being displayed on the absorption spectrum. This therefore means that forbidden transitions are those that would mean there is no change in the angular momentum quantum number, ℓ. If $\Delta\ell$=0, the transition is

forbidden. However, if $\Delta \ell = +/-1$, a dipole moment is created in the transition and so the transition is allowed.

2.7   Polarisation

This section discusses the concept of polarisation, including the properties of polarisers and half-wave plates - both of which are vital components used in the experimental setup for this thesis.

Being an electromagnetic wave, light has magnetic field and electric field components which oscillate perpendicular to the direction of propagation and to each other. Polarisation refers to the orientation and oscillation of the electric field component of light and sources can either be polarised, as with laser light, or unpolarised, as with sunlight. Light is polarised depending on the orientation of the electric field. It can be either linearly, circularly or elliptically polarised.

Linear polarisation describes the electric field of light oscillating in one plane, as shown in Figure 2.25.
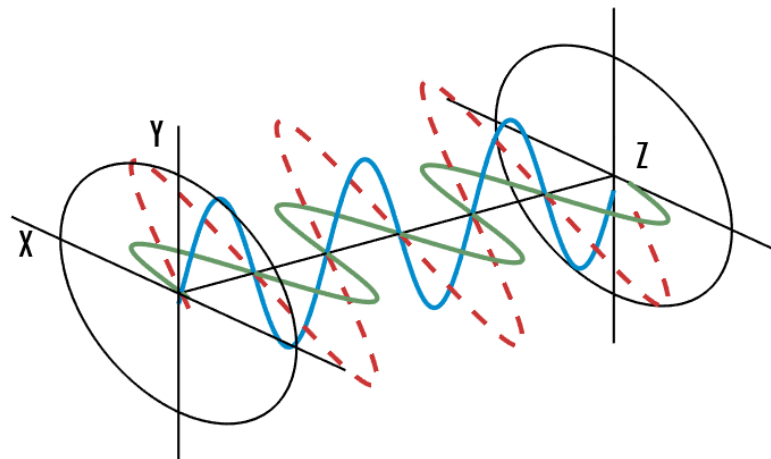
Figure 2.25: The electric field of linearly polarised light (red) with components (blue/green) that have no phase difference. [39]

The resulting electric field propagates linearly, as shown by the red dotted line, due to equal amplitudes and no phase difference between the two electric field components.

Circular polarisation describes the electric field of light consisting of two perpendicular linear components that are equal in amplitude but have a phase difference of 90°, as shown in Figure 2.26.
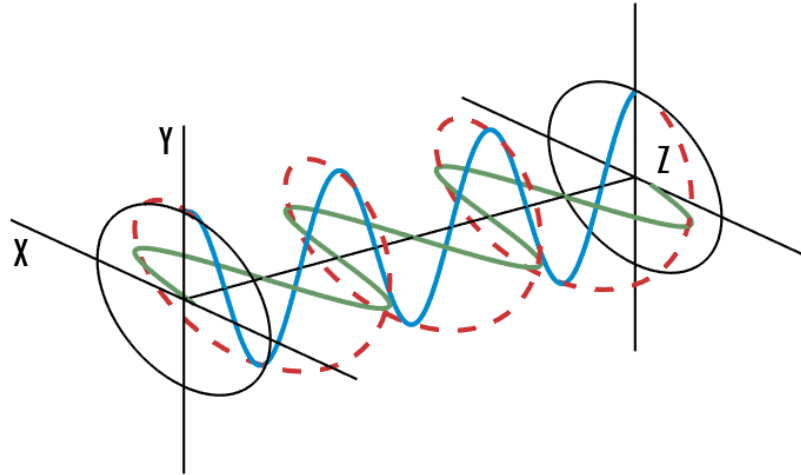
Figure 2.26: The electric field of circularly polarised light (red) with components (blue/green) that have a phase difference of 90°. [39]

The resulting electric field propagates circularly as shown by the red dotted line due to the phase difference.

Elliptical polarisation describes the electric field of light consisting of two perpendicular linear components that either have a phase difference other than 90° or have different amplitudes, as shown in Figure 2.27.
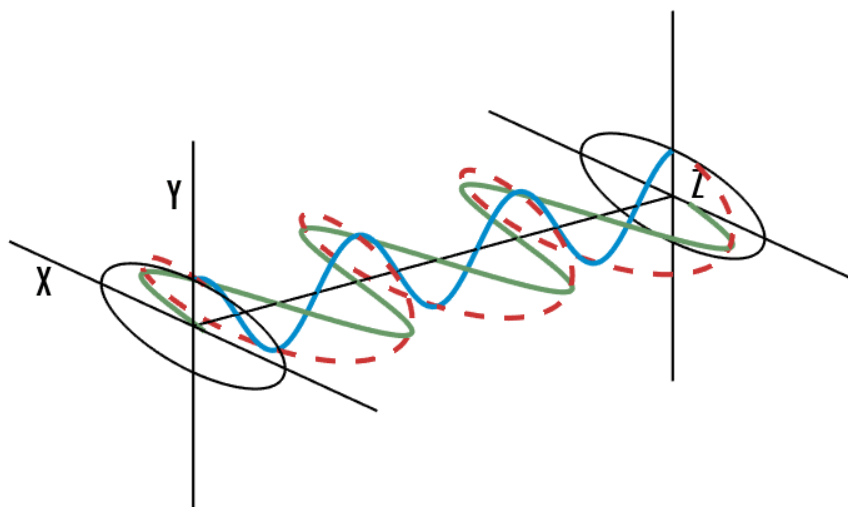
Figure 2.27: The electric field of elliptically polarised light (red) with components (blue/green) that have different amplitudes. [39]

The resulting electric field propagates elliptically as shown by the red dotted line due to the difference in amplitudes.

2.7.1   Polarisers

Polarisers are optical devices that can be used to convert unpolarised light into a form of polarised light. For the purposes of this thesis, we only need consider linear polarisers, which convert unpolarised light into linearly polarised light.
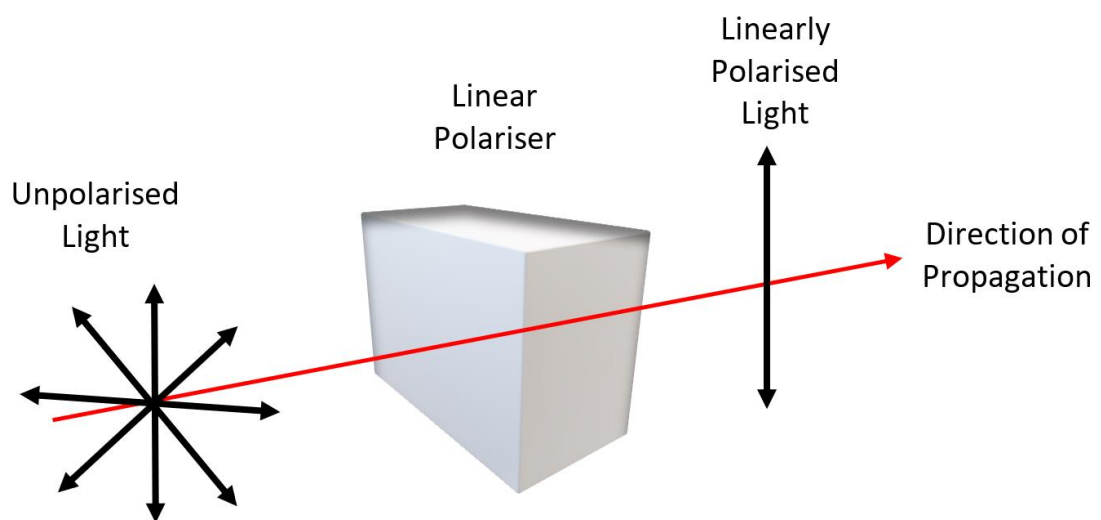
Figure 2.28: A schematic diagram demonstrating how a linear polariser can be utilised to convert unpolarised light to linearly polarised light.

Figure 2.28 illustrates the function of a linear polariser. It filters out all oscillations of electric field except for in one plane. In the case of Figure 2.28, the linear polariser is oriented vertically so as to only allow vertical oscillations to pass through, absorbing the light in all other planes.

2.7.2   Waveplates

Waveplates are an optical device that can be used to either change the polarisation state or rotate the direction of polarisation – they have no effect on unpolarised light. Waveplates consist of two axes, a slow axis and a fast axis, that are perpendicular to

each other and to the direction of propagation of the incoming wave. They work by delaying one component of the polarisation, since the birefringent material they are made from cause different orientations of polarised light to experience different refractive indices. Light that is polarised along the slow axis experiences a high refractive index and travels slower than light polarised along the fast axis which experiences a lower refractive index and travels faster than the slow axis, but still slower than the incident light.

Used in the experimental section of this thesis, half-waveplates can be used to rotate the polarisation of linearly polarised light, which has been previously polarised using a linear polariser, as shown in Figure 2.29. Other waveplates, however, such as a quarter-waveplate can be used to convert linearly polarised light into circularly polarised light.
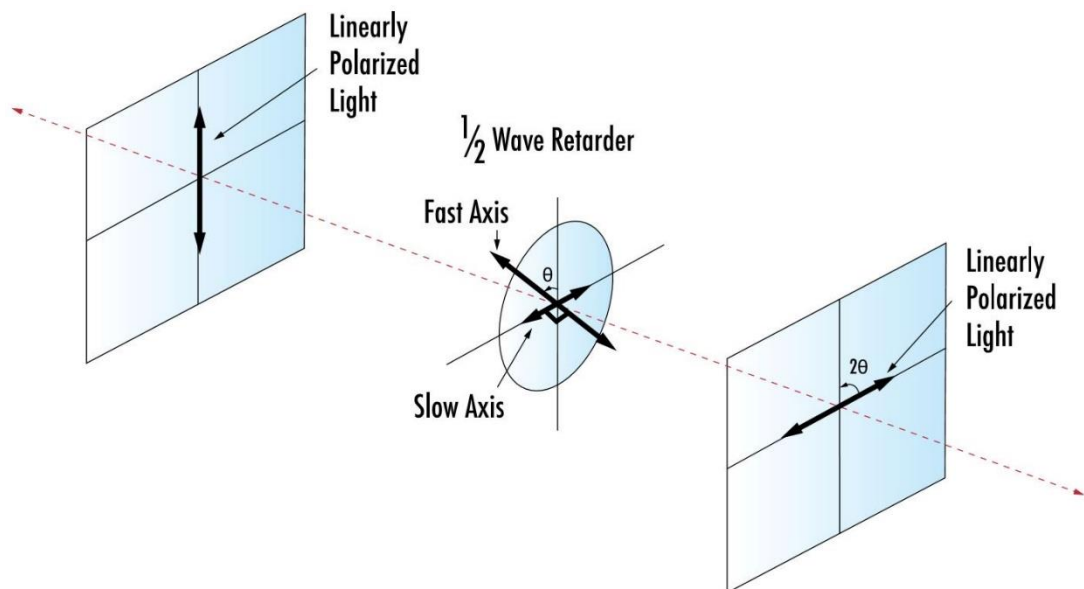
Figure 2.29: Using a half-waveplate to rotate the plane of polarisation of linearly polarised light. [(40)]

Figure 2.29 demonstrates how a half-wave plate can be used to re-orientate linearly polarised light from vertical to horizontal plane polarisation. This can be particularly

useful when working with lasers, which are typically horizontally polarised and so waveplates can be used to alter to a desired orientation. The waveplate can be attached to a manual rotation mount and for every 1° of rotation of the waveplate, the angle of polarisation rotates 2°. Therefore, over through a 180° rotation of the waveplate, we expect to see two maxima and two minima intensity peaks, since this corresponds to 360° rotation of polarisation.

3   Methodology

This chapter outlines the methods behind the synthesis of each component of the NU-1000 MOF used in this study, including information on the preparation of the samples used. It concludes by outlining the methodology behind collection of results and set-up design.

3.1   Ligand and Subsequent MOF Synthesis

The method of synthesis of the NU-1000 MOF was carried out with reference to previous research conducted by Wang et al. 2015[41]. This involves a two-step synthesis of the organic linker and then a further synthesis to produce NU1000.
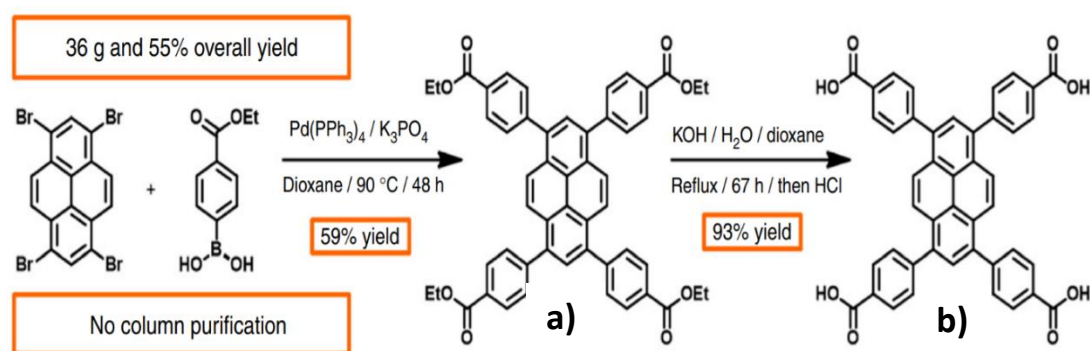
Figure 3.1: Two-step synthesis process of the NU-1000 ligand H4TBAPy. [41]

The aforementioned two-step process is depicted in Figure 3.1. The first step involves synthesising the ligand 4,4`,4'',4'''-(pyrene-1, 3,6,8-tetrayl) tetrabenzoic acid by a reaction between the pyrene 1,3,6,8-tetrabromopyrene and ethyl ester (4-(ethoxycarbonyl)phenyl) boronic acid. This ethyl ester is used in order to slow down the hydrolysis of the benzoic ester, avoiding a mixture of mono, bis, tris and tetra benzoic acids forming [41]. Filtration provides the tetraester (Figure 3.1a). The second

step is to hydrolyse, under reflux, the tetraester to provide the tetra-acid (Figure 3.1b) – the required ligand for use in the synthesis of NU-1000 [41].
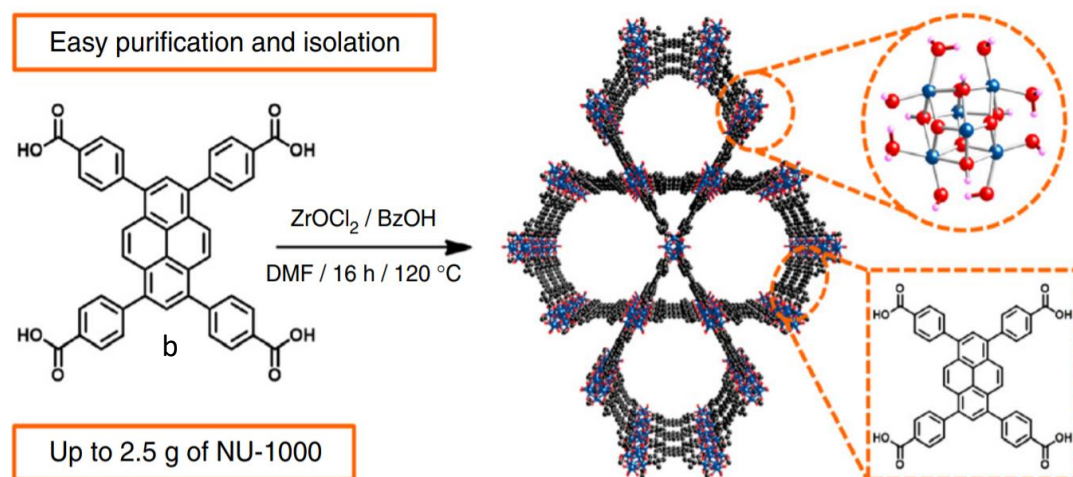
Figure 3.2: Process for synthesising NU-1000 from the tetra-acid ligand H4TBAPy. [41]

Figure 3.2 demonstrates how the previously synthesised ligand is used for synthesis of NU-1000. NU-1000 is synthesised from this ligand, zirconyl chloride ($ZrOCl_2$) and benzoic acid (BzOH) as a moderator in N,N – dimethylformamide (DMF) [41]. The moderator is then removed by washing with a HCl solution and thermally activated to remove excess solvent [41].

3.2   Sample Preparation

Two forms of samples were prepared – MOFs in a capillary suspended in bromobenzene and MOFs dispersed in resin, oriented by magnetic field, then fixed in place by resin curing. The reason for alignment of the MOFs is because it creates a well-defined orientation for the transition dipole moments, as opposed to random orientation where the dipole moments are averaged at the collection point. We

would therefore expect to experience an increase intensity of measured fluorescence when the MOFs are aligned.

3.2.1 NU-1000 Modification

In order to ensure that a stable suspension of MOFs is formed in bromobenzene, the NU-1000 was functionalized with trimethoxy(octadecyl)silane (TMODS) to produce NU-1000$_{Si}$, which disperses more readily and does not sediment as rapidly.

3.2.2 MOF Suspension Samples

In order to prepare the suspension of NU-1000$_{Si}$ (1.29mg) in bromobenzene (0.865mL), they were added together and sonicated for 60 seconds until there was a homogenous suspension (0.1%). The capillary cell was dipped into the NU-1000$_{Si}$ suspension mixture so as to fill it through capillary action, then sealed with UV-glue. To prepare the sample, the capillary was constructed by coating each side with 3nm of chromium then 7nm of gold. This will act as the electrodes once connected to silver wires attached to a wave function generator and oscilloscope in order to control the strength of the applied electric field.

3.2.2.1 *CCD Images of NU-1000$_{Si}$ Microrod Alignment*

The images in Figure 3.3, taken using a Thorlabs DCC1645C Compact CMOS camera, show a difference in orientation of the microrods. Figure 3.3a shows microrod orientation without the presence of an electric field, demonstrating unalignment and random orientation in all directions. This is shown by dots – microrods facing out of the page- and dashes – microrods facing across the page. Figure 3.3b demonstrates how the microrods align with the presence of an external electric field, with much more order and similar orientation to each other. The microrods here are shown to

be aligned with their major axes facing out of the page, hence they are seen as dots as opposed to dashes. This gives rise to the lower light intensity seen. These images can be used as visible proof and further evidence, alongside the measurements taken, that the MOF orientation can be altered by an external field.

a)

b)
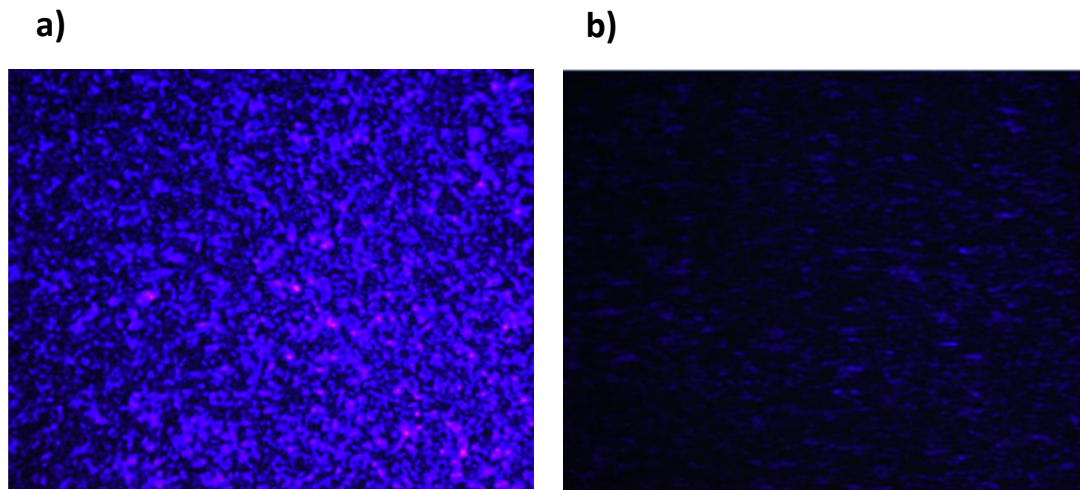
Figure 3.3: CCD images of a) unaligned and b) aligned MOFs in suspension sample.

3.2.3 MOF Resin Samples

The resin samples were prepared by dispersing the NU-1000$_{Si}$ microrods in clear resin - 3 variations of this sample were prepared.
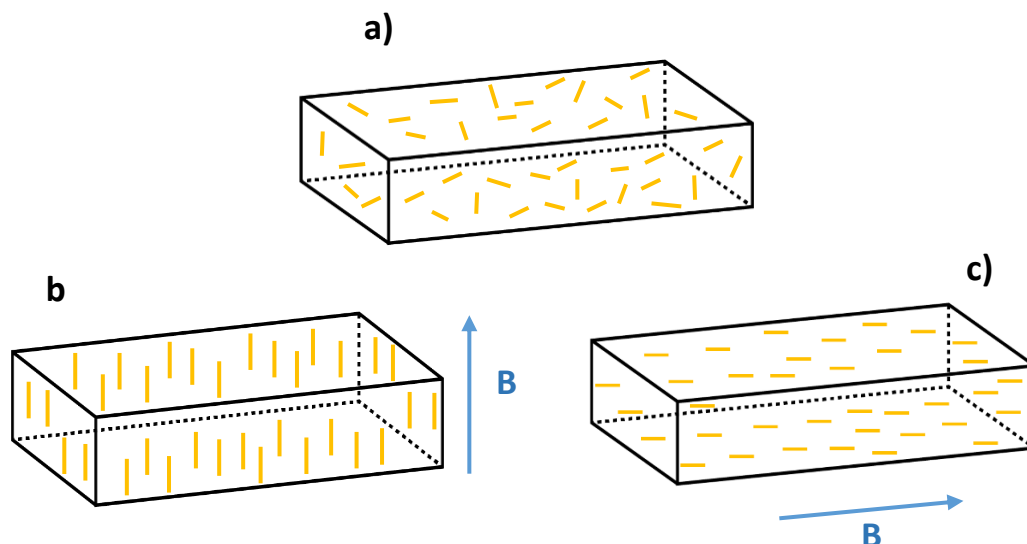
Figure 3.4: Prepared resin samples with a) random, natural orientation and magnetic b) vertical alignment and c) horizontal alignment. Sample dimensions are 2 x 6 x 20mm. 'B' indicates direction of applied magnetic field.

The difference in MOF orientation and alignment between the three samples is shown in Figure 3.4. Figure 3.4a shows random orientation and no alignment and is the sample that was left natural and unmagnetized. Figures 3.4b and 3.4c show the microrods possessing vertical and horizontal alignment respectively due to a neodymium magnet being held at a distance of 6cm above and to the side of the sample respectively. They show the microrods aligning with the magnetic field direction.

The microrods aligned themselves along the direction of the applied magnetic field. The resin was then photocured to fix the MOFs in place. Therefore, we now had samples that are pre-aligned, by magnetic field, samples ready to be aligned by electric field and samples that can be left unaligned. This should allow us to confirm our aims and determine if there is any correlation between the fluorescence of the MOFs and the angle of polarisation relative to the MOF crystal orientation.

3.3   Fluorescence Spectra

Fluorescence spectra of the NU-1000 MOF and used solvent, in Figure 3.5, indicate where the emission peaks appeared when excited with a 405nm laser.
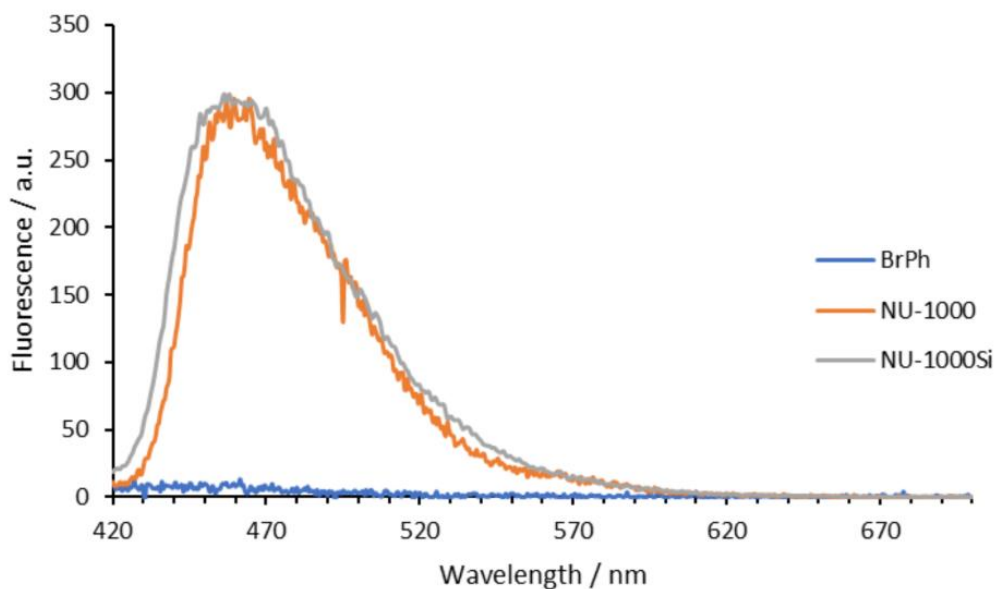
Figure 3.5: Fluorescence spectra of NU-1000$_{Si}$ (grey) and bromobenzene solvent (blue). Also includes the unmodified NU-1000 (orange).

It demonstrates an emission peak of NU-1000$_{Si}$ at a wavelength of around 460nm and shows how little the solvent, bromobenzene (BrPh), fluoresces and affects results. The bromobenzene spectrum was taken with the solvent in an empty capillary and will be used as a background and taken from all results so that the fluorescence measured is purely from the MOFs.

3.4   Setup Design – Polarisation of Absorption

In order for excitation and subsequent fluorescence of the MOFs to occur we used a 405nm blue laser, with the fluorescence measured using a spectrometer reading back to a computer. The explanation for the use of each component in the setup seen in Figure 3.6 is outlined below.
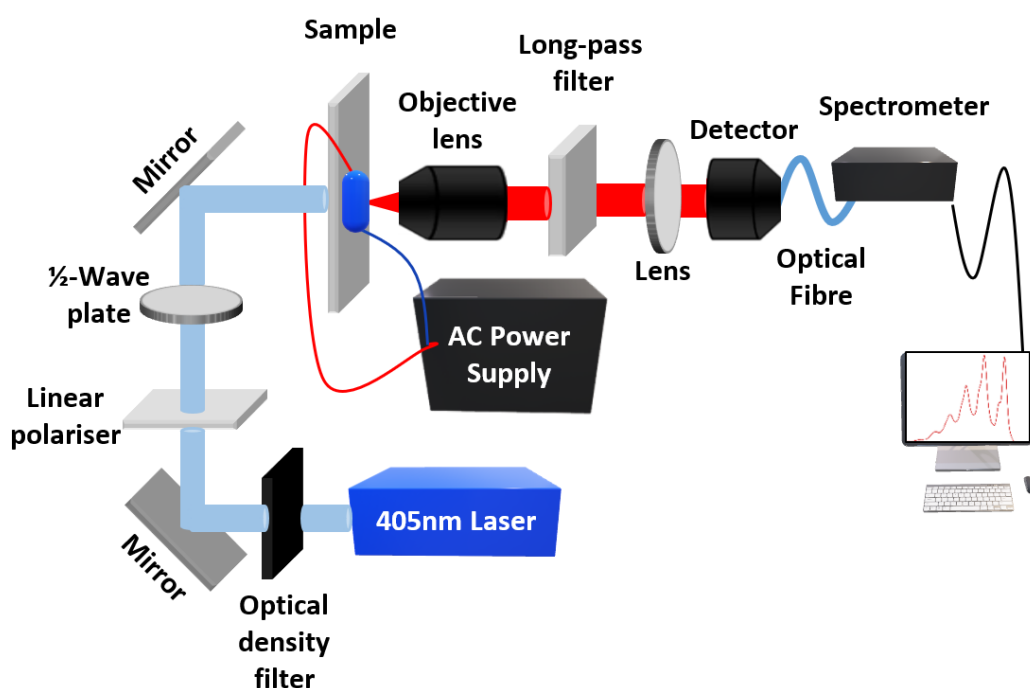
Figure 3.6: Fluorescence-measuring setup for polarisation of absorption.

The variable neutral optical density filter allows for control of the laser intensity without altering the current flowing through the laser diode, ensuring greater stability of laser emission intensity over time. It was particularly used to reduce the intensity so as to not saturate the measurements or cause photobleaching of the sample. The linear polariser cleans the polarisation, ensuring a clean linearly polarised beam, with the half-waveplate allowing for control of rotation of the

polarisation. The fluorescence was collected using a 10X magnification Mitutoyo Plan Apo infinity corrected long working distance objective lens (20mm effective focal length). Once collected, the long-pass filter removes the unwanted laser excitation wavelength, removing wavelengths shorter than 437nm. The final lens (400mm focal length) couples into the optical fibre. This optical fibre (200μm diameter) is used to waveguide the signal to an Avantes AvaSpec-ULS3648 fibre optic spectrometer. This data was then sent to a computer and interpreted using AvaSoft spectrometer software.

A manually controlled shutter was also placed in the setup directly prior to the laser beam reaching the sample. This was closed between each measurement to reduce unnecessary light exposure to the samples, reducing the likelihood of photobleaching occurring.

As a result of the product of the optical fibre diameter and microscope objective effective focal length divided by the lens focal length, the collection area on the sample corresponds to a disk of 40μm in diameter. As seen previously, in Figure 2.13, the microrods are around 5μm in length, meaning the collection area is much larger than a single MOF. This therefore means that fluorescence collected will be from a multitude of MOFs, rather than a single MOF.

3.4.1   Methodology

The samples were illuminated with a 405nm laser, set at a power of around 3mW, with measurements taken at 5^0 increments upon rotation of the half-waveplate, up to 180°. This represents measurements of incident polarisation rotating in 10^0 increments from 0^0 through to 360°. For each taken measurement, the spectrometer

had an integration time of 5 seconds to allow sufficient collection of fluorescence. This was done for aligned and unaligned resin samples.

Results were plotted by integrating the fluorescence intensity with respect to wavelength and normalising its value against the maximum recorded intensity value. All of the results taken show a slight tilt of around 10° – the maxima and minima values do not perfectly correspond to 0^0 and 45° respectively on the polariser. This is due to the incorrect configuration of the polariser. The numbers represented on the manually turned wheel were not a precise representation of the angle of polarisation, but were around 12° different. This explains the discrepancies in results.

For the suspension MOF samples, an AC supply was attached and measurements taken with and without an applied voltage (100V, 500Hz) as to determine the difference in measured fluorescence between aligned and unaligned MOFs and demonstrate dynamic electric field alignment of MOFs. The distance between the electrodes is 1mm.

3.5   Setup Design - Polarisation of Emission

In this section, we demonstrate how the measured fluorescence of the NU-1000$_{Si}$ MOF differs depending on the MOF crystal orientation and polarisation of the emitted beam from the fluorescence of the samples. This is in order to determine any preferentiality between emission and absorption polarisations of the MOFs.
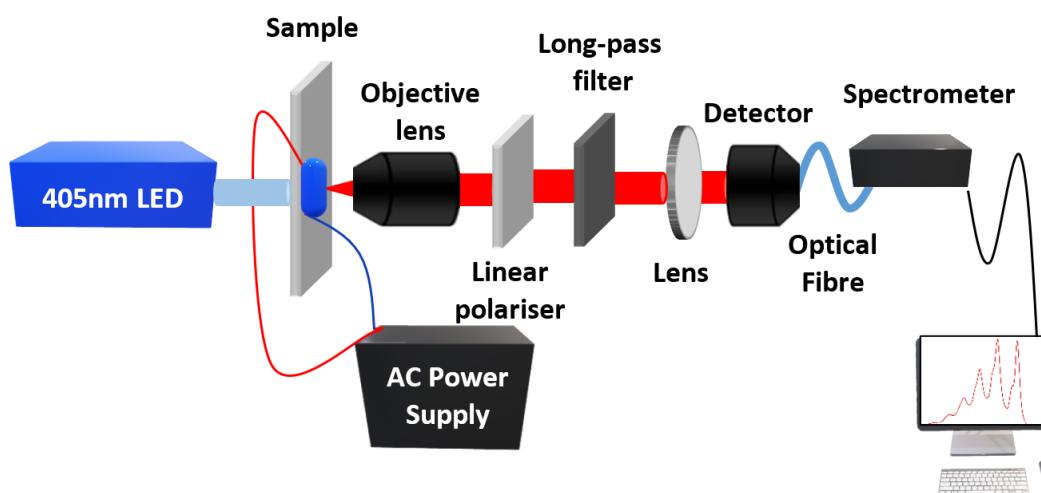
Figure 3.7: Fluorescence-measuring setup for polarisation of emission.

The main alteration of the setup for this section is the source. Rather than a laser source we changed to an Opulent Americas Luminus SST-10-UV-A130 405nm UV LED, in order to provide a source which is unpolarised, unlike a laser which is typically linearly polarised meaning that the light from the LED is collimated onto the sample. For this set of experiments, we are probing the polarisation state of emission. We therefore no longer need the half-waveplate as the polariser allows for control of polarisation state, only allowing certain polarisations to pass through. The LED power supply was set to 3.6V and 1.4A. The methodology for collection and plotting of results remains identical to that used for polarisation of absorption.

4 Results and Discussion

This Chapter presents and discusses the results collected from experiments of polarisation of absorption and polarisation of emission.

4.1 Polarisation of Absorption

In this section, we demonstrate how the measured fluorescence of the NU-1000$_{Si}$ MOF differs depending on the MOF crystal orientation and polarisation of the transmission beam from the blue laser.

4.1.1 MOFs fixed in resin

This section separates the three resin samples and presents the results in terms of whether the MOFs were left unaligned or magnetically aligned either vertically or horizontally. The predicted difference in results will tell us if the direction of alignment or lack of orientation has any effect on the measured fluorescence intensity. It will also tell us, primarily, if the MOFs can actually be magnetically aligned, as they should theoretically be able to, due to differences in the measurements.

4.1.1.1 Unaligned MOFs

The first measurements were taken from the resin sample of unaligned MOFs as previously shown in Figure 3.4a.
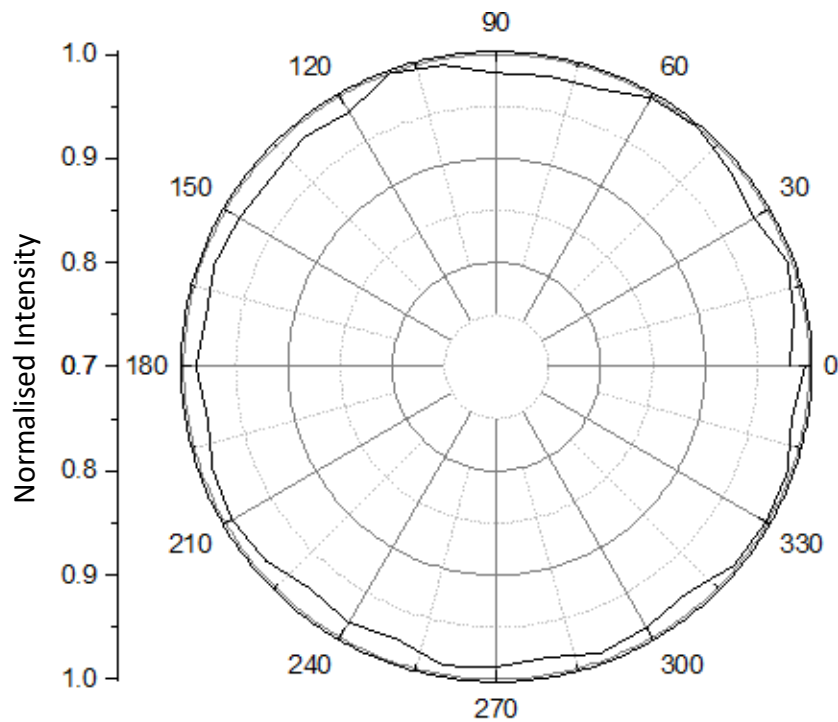
Figure 4.1: Unaligned resin sample measurements (absorption polarisation).

The intensity of emission, represented by normalised intensity on the y axis, is directly proportional to the number of absorbed photons. The number of absorbed photons depends on the transition dipole moment of the MOFs. Since the intensity, and therefore number of absorbed photons, remains almost constant at each angle of polarisation, there is an averaging of the transition dipole moments orientation occurring. As a result, it is determined that there is no alignment of the MOF, as the results show random orientation, as expected.

The results shown by the plot in Figure 4.1 indicate that altering the polarisation angle does not affect the measured intensity of fluorescence from the unaligned resin MOF sample. This is due to there being no preferential absorption direction with respect to incident polarisation.

Next are the measurements taken for the MOFs aligned vertically, as previously shown in Figure 3.4b.
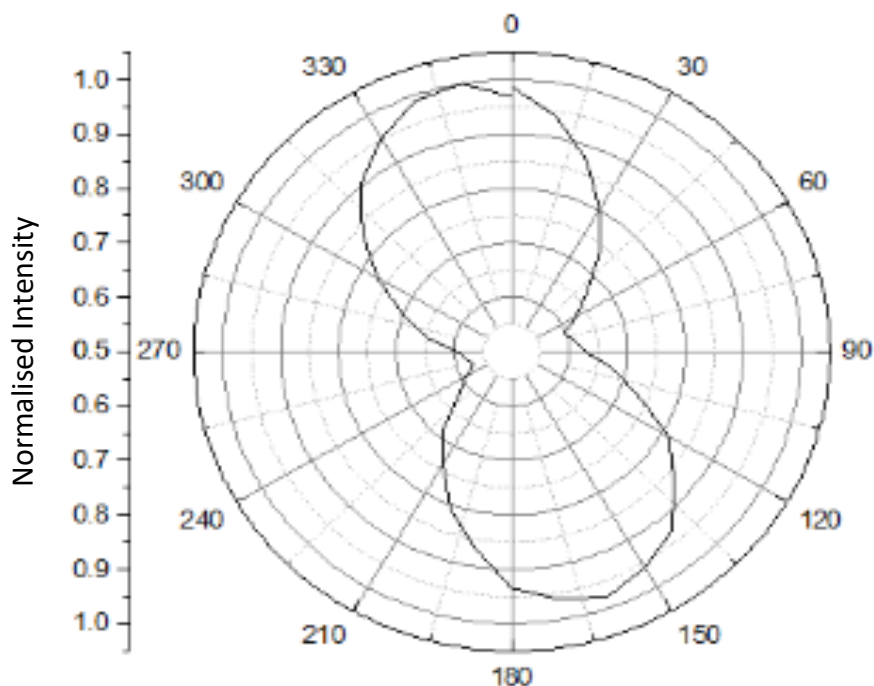
Figure 4.2: Vertically aligned resin sample measurements (absorption polarisation).

The vertically aligned MOFs demonstrates minimum and maximum intensity at different angles of polarisation. The MOFs are aligned parallel to the direction of the source of excitation, along their major axes. This suggests that there is a preferential alignment of MOF orientation. This, along with a well-defined absorption dipole transition moment, corresponds to an anisotropy in absorption as a function of the angle of polarisation.

4.1.1.3 Horizontally aligned MOFs

Finally, for the resin samples, we study the measurements taken for the horizontally aligned MOFs as previously shown in Figure 3.4c.
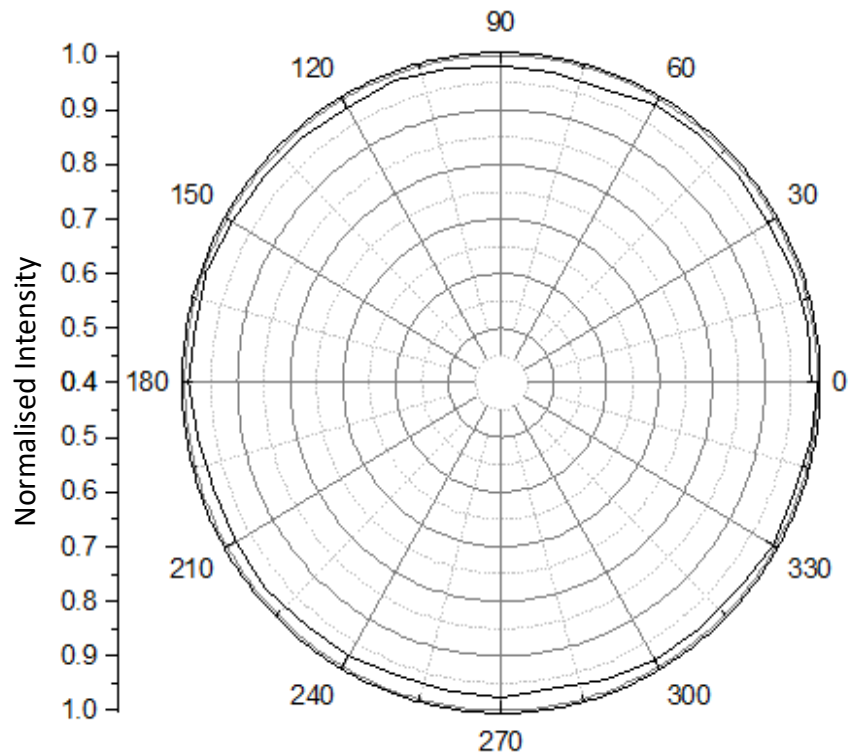
Figure 4.3: Horizontally aligned resin sample measurements (absorption polarisation).

The horizontally aligned MOFs demonstrate an averaging of the transition dipole moment orientation, similar to that of the unaligned MOFs, shown in Figure 4.3. The MOFs are aligned perpendicular to the direction of the source of excitation, along their minor axes, hence a response similar to unaligned MOFs. They have no response to polarisation angle since they are not aligned with their major axes parallel to detection direction.

4.1.2   MOF suspension sample

Results for the MOF suspension sample are shown in Figure 4.4. Measurements taken without an applied electric field are in red, while those taken with an A.C electric field applied are in blue. These measurements were all taken on the same sample of MOFs suspended in bromobenzene.
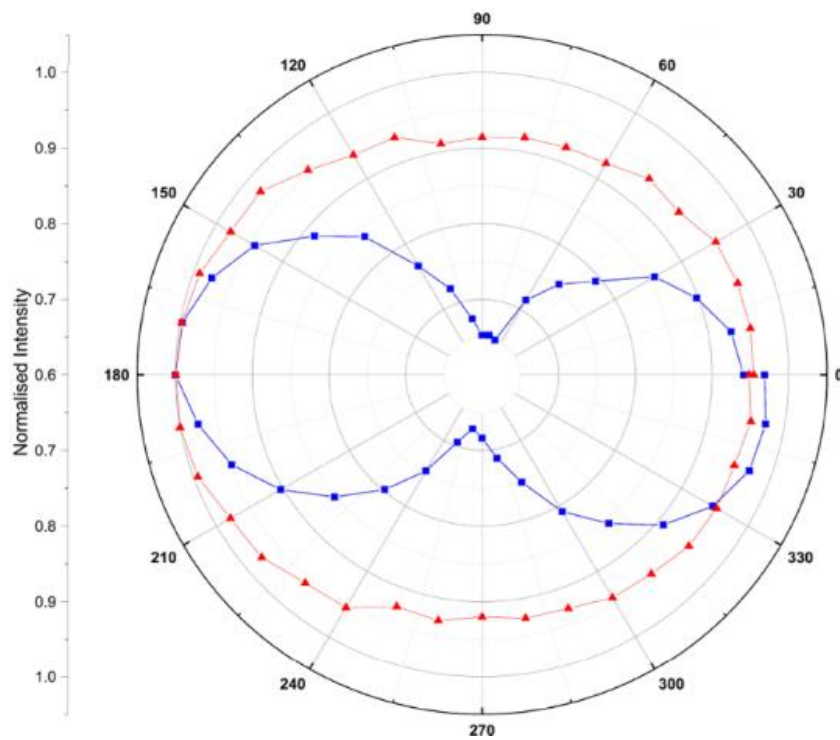
Figure 4.4: MOF suspension sample measurement (absorption polarisation).

The suspension of MOFs without an electric field applied demonstrated a relatively constant intensity of absorbed photons similar to that seen by the unaligned resin samples. When an electric field was applied, the results showed a figure-of-eight pattern, with minimum fluorescence intensity occurring at polarisation angles of 45°, 135°, 225° and 315° and maximum fluorescence occurring at polarisation angles of 0°/360°, 90°, 180° and 270°, which correspond to the minimum and maximum angles of polarisation on the polariser. These results are similar to those seen in the vertically aligned resin samples. This suggests that the application of an electric field is responsible for the alignment of the MOFs.

Moreover, after having aligned the MOFs with an electric field, the MOFs would return to random orientation/unalignment once the electric field was removed. This

demonstrates the reversibility and repeatability of these MOFs in a suspension sample – they can be aligned and unaligned as required.

4.2   Polarisation of Emission

4.2.1   MOFs fixed in resin

The resin samples used in this section are the exact same as those used in section 4.1. These results were taken to determine whether there is a preferential polarisation state and if there is preferentiality between polarised emission or absorption.

4.2.1.1   4.2.1.1 Unaligned MOFs
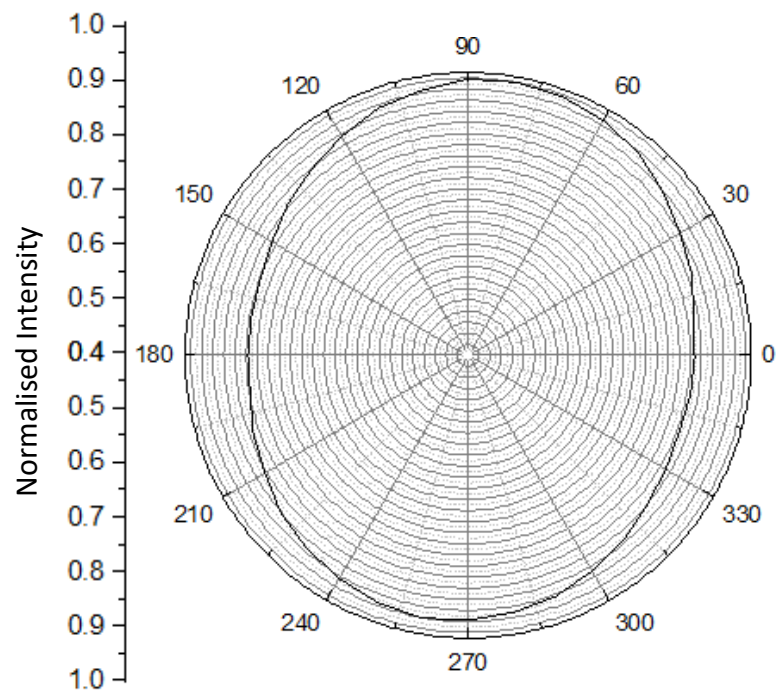
Figure 4.5: Unaligned resin sample measurements (emission polarisation).

The plot in Figure 4.5 displays similar results to those seen by the unaligned resin samples for polarisation of absorption – there is an averaging of the transition dipole moments, proving there is, again, no overall alignment.

4.2.1.2   Vertically aligned MOFs
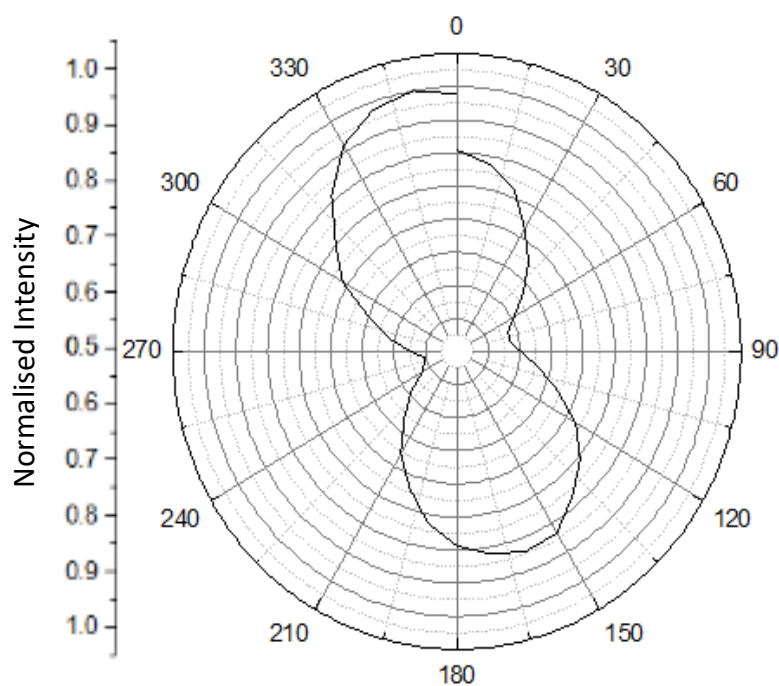
Figure 4.6: Vertically aligned resin sample measurements (emission polarisation).

Again, the results in Figure 4.6 demonstrate similar results to those seen by the vertically aligned resin samples for polarisation of absorption – there is a well-defined transition dipole moment.

4.2.1.3   Horizontally aligned MOFs

Likewise, for the following results – they are similar to those taken by the horizontally aligned resin samples for polarisation of absorption. Since the MOFs are aligned perpendicular to the viewing direction, there is no response to varying polarisation, shown in Figure 4.7.
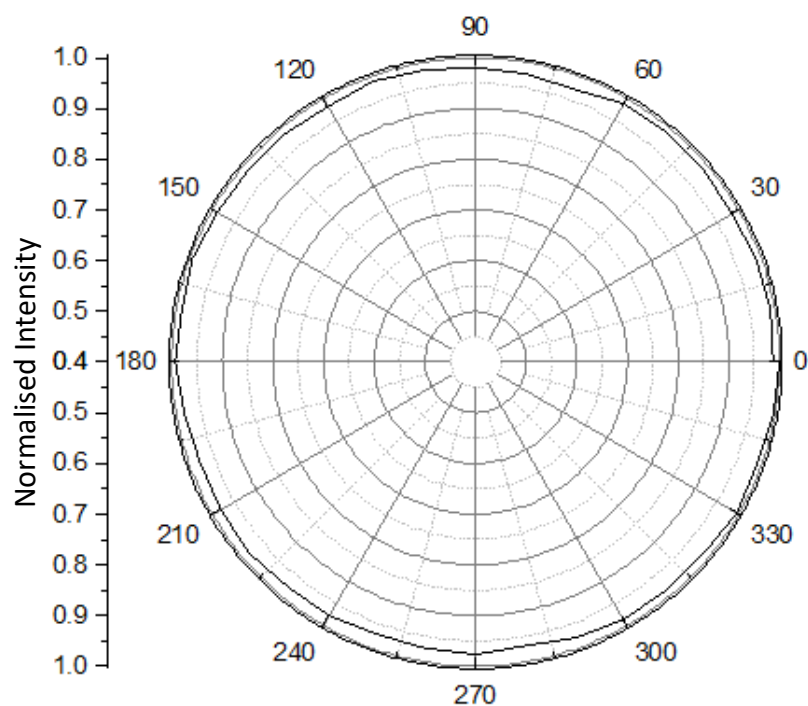
Figure 4.7: Horizontally aligned resin sample measurements (emission polarisation).

4.2.2   MOFs suspended in bromobenzene

Since we know that the MOFs can be successfully aligned, we can probe the polarisation state of the fluorescence.
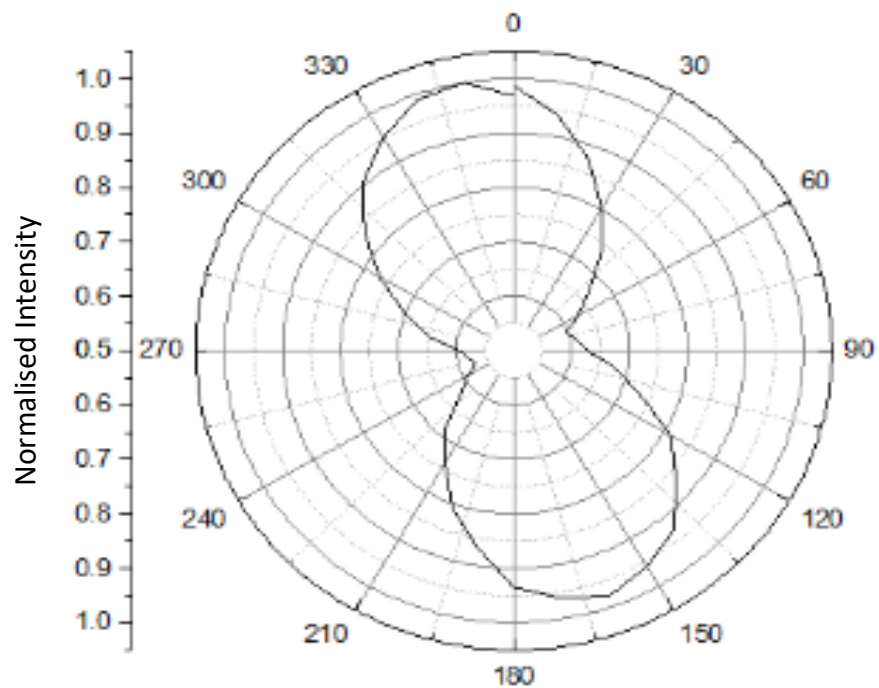
Figure 4.8: MOF suspension sample measurements (emission polarisation).

The results in Figure 4.8 demonstrate a polarised emission. It is therefore possible, by controlling the orientation of the microcrystals, to dynamically control the polarisation state of the emission.

5   Conclusions, Applications and Future Work

This final chapter brings together all the work and results presented in this thesis and draws conclusions based on the research conducted. The conclusions that are drawn, given that the thesis aims and objectives were met, will give rise to potential new applications for the NU-1000$_{Si}$ MOF and MOFs with similar anisotropic properties and are outlined below. Due to the success of this research, we also suggest future work that may be of interest.

5.1   Conclusions

To summarise, it is evident that the orientation of the NU-1000$_{Si}$ MOF can be manipulated by use of electric and magnetic fields in order to induce alignment. It is also possible, given that there is a polarised emission, to dynamically control the polarisation state of the emission.

Previous work, as conducted by Cheng, F et al [4], demonstrated the dynamic alignment of NU-1000$_{Si}$ via magnetic fields. However, the ability to use electric fields for alignment proves much more useful due to its simplicity and greater application benefits. The ease of use of electric fields is due to the larger dynamic range of field strengths and ease of localisation.

5.2   Potential Current and Future Applications

Due to the optoelectrical response to linearly polarised UV light demonstrated by the NU-1000$_{Si}$ MOF, there is potential for the use as an optical switch because of their reversibility. The rods can be aligned and unaligned, or aligned in different directions, to 'turn' on and off a switch.

They also have potential for uses as active sensors and use in displays due to their reversibility.

5.3 Potential Future Work

Due to the success of the experiments outlined in this thesis, we have ideas for some potential future work. The measurements we took were all from samples of an ensemble of MOFs. It may prove useful to alter the setup by replacing the objective lens with a one of higher magnification in order to perform measurements on single MOFs. This will allow the study of the anisotropic properties of a single MOF and the fluorescent properties of individual MOFs. Such experiments could also be carried out in an attempt to dynamically align other MOFs via electric field.

References

1. Ohhashi, T., Tsuroka, T., Fujimoto, S., Takashima Y. & Akamatsu K., 2017. *Controlling the Orientation of Metal-Organic Framework Crystals by an Interfacial Growth Approach Using a Metal Ion-Doped Polymer Substrate.* American Chemical Society, 18(1), 402-408.
2. Falcaro, P., Ricco, R., Doherty, C.M., Liang, K., Hill, A.J., Styles, M.J., 2014. *MOF positioning technology and device fabrication.* Chemical Society Reviews, 43(16), 5513-5560.
3. Ikigaki, K., Okada, K., Tokudome, Y., Toyao, T., Falcaro, P., Doonan, C.J. & Takahashi, M., 2019. *MOF-on-MOF: Oriented Growth of Multiple Layered Thin Films of Metal-Organic Frameworks.* Angewandte Chemie, 50(21), 6886-6890.
4. Cheng, F., Marshall, E.S., Young, A.J., Robsinon, P.J., Bouillard, J-S. G, Adawi, A.M., Vermeulen, N.A., Farha, O.K., Reithofer, M.R. & Chin, J.M., 2017. *Magnetic Control of MOF Crystal Orientation and Alignment.* Chemistry – A European Journal, 23(62), 15578-15582.
5. Seyyedi, B. & Bordiga, S., 2015. *Metal-Organic Frameworks: A New Class of Crystalline Porous Materials.* Johnson Matthey Technology Review, 59(2), 123-125.
6. Akinola, T.O., 2016. *Processing and Patterning of Metal Organic Frameworks and Metal Organic Gels.* [Master's Thesis]. The University of Hull.
7. Kramer, K., 2017. *MOFs: Metal-organic frameworks.* ChemistryWorld [Podcast]. 27 April.
8. Yaghi, O.M., O'Keeffe, M., Ockwig, N.W., Chae, H.K., Eddaoudi, M. & Kim, J., 2003. *Reticular synthesis and the design of new materials.* Nature, 423, 705-714.
9. Millward, A.R. & Yaghi, O.M., 2005. *Metal-Organic Frameworks with Exceptionally High Capacity for Storage of Carbon Dioxide at Room Temperature.* Journal of The American Chemical Society, 127(51), 17998-17999.
10. Berger, M., 2019. *What is a MOF (metal organic framework)?* Nanowerk, Available online.
11. Butova, V.V., Soldatov, M.A., Guda, A.A., Lomachenko, K.A. & Lamberti, C., 2016. *Metal-organic frameworks: structure, properties, methods of synthesis and characterization.* Russian Chemical Reviews, 85(3), 280.
12. Rowsell, J.L.C. & Yaghi, O.M., 2004. *Metal-organic frameworks: a new class of porous materials.* Microporous and Mesoporous Materials, 73(1-2), 3-14.
13. Grace, W.R. & Co., 2017. *Synthetic Non-fibrous Zeolites Product Stewardship Summary*. Grace, Available online.
14. novoMOF, 2019. *Metal-Organic Frameworks.* Available online.
15. Glover, T.G., Peterson, G.W., Schindler, B.J., Britt, D. & Yaghi, O.M., 2010. *MOF-74 building unit has a direct impact on toxic gas adsorption.* Chemical Engineering Science, 66(2), 163-170.

16. Li, H., Wang, K., Sun, Y., Lollar, C.T., Li, J. & Zhou, H-C., 2018. *Recent advances in gas storage and separation using metal-organic frameworks.* Materials Today, 21(2), 108-121.
17. Thonhauser, T., Zuluaga, S., Arter, C.A., Berland, K., Schröder, E. & Hyldgaard, P., 2015. *Spin Signature of Nonlocal Correlation Binding in Metal-Organic Frameworks.* Physical Review Letters, 115(13), 136402.
18. Lee, J-H., Nguyen, T-B., Nguyen, D-K., Kim, J-H., Kim, J-Y., Phan, B.T. & Kim, S.S., 2019. *Gas Sensing Properties of Mg-Incorporated Metal-Organic Frameworks.* Sensors, 19(15), 3323.
19. Xu, G., Nie, P., Dou, H., Ding, B., Li, L. & Zhang, X., 2017. *Exploring metal organic frameworks for energy storage in batteries and supercapacitors.* Materials Today, 20(4), 191-209.
20. Sert, E., Yilmaz, E. & S. Atalay, F., 2017. *Comparison of Solvothermal and Ionothermal Methods on Catalytic Activity of MIL-53 (Fe).* Anadolu University Journal of Science of Science and Technology, 18(5), 1107-1117.
21. Leo, P., Orcajo, G., Briones, D., Calleja, G., Sánchez-Sánchez, M. & Martínez, F., 2017. *A Recyclable Cu-MOF-74 Catalyst for the Ligand-Free O-Arylation Reaction of 4-Nitrobenzaldehyde and Phenol.* Nanomaterials, 7(6), 149.
22. Katz, M.J., Howarth, A.J., Moghadam, P.Z., DeCoste, J.B., Snurr, R.Q., Hupp, J.T. & Farha, O.K., 2016. *High volumetric uptake of ammonia using Cu-MOF-74/Cu-CPO-27.* Dalton Transactions, 45(10), 4150-4153.
23. Flores, J.G., Sánchez-González, E., Gutiérrez-Alejandre, A., Aguilar-Pliego, J., Martínez, A., Jurado-Vázquez, T., Lima, E., González-Zamora, E., Díaz-García, M., Sánchez-Sánchez, M. & Ibarra, I.A., 2018. *Greener synthesis of Cu-MOF-74 and its catalytic use for the generation of vanillin.* Dalton Transactions, 47(13), 4639-4645.
24. Remya, V.R, & Kurian, M., 2018. *Synthesis and catalytic applications of metal-organic frameworks: a review on recent literature.* International Nano Letters, 9, 17-29.
25. Islamoglu, T., Otake, K-i., Li, P., Buru, C.T., Peters, A.W., Akpinar, I., Garibay, S.J. & Farha, O.K., 2018. *Revisiting the structural homogeneity of Nu-1000, a Zr-based metal-organic framework.* CrystEngComm, 20(39), 5859-6096.
26. US Department of Energy, 2017. *Metal-organic framework NU-1000 allows separation of toxic furanics from sugars for efficient ethanol production.* Available online.
27. Hod, I., Deria, P., Bury, W., Mondloch, J.E., Kung, C-W., So, M., Sampson, M.D., Peters, A.W., Kubiak, C.P., Farha, O.K. & Hupp, J.T., 2015. *A porous proton-relaying metal-organic framework material that accelerates electrochemical hydrogen evolution.* Nature Communications, 6, 8304.
28. Liu, W-G. & Truhlar, D.G., 2017. *Computational Linker Design for Highly Crystalline Metal-Organic Framework NU-1000.* Chemistry of Materials, 29(19), 8037-8081.

29. Planas, N., Mondloch, J.E., Tussupbayev, S., Borycz, J., Gagliardi, L., Hupp, J.T., Farha, O.K. & Cramer, C.J., 2014. *Defining the Proton Topology of the Zr_6-Based Metal-Organic Framework NU-1000.* The Journal of Physical Chemistry Letters, 5(21), 3716-3723.
30. Ning, D., Liu, Q., Wang, Q., Du, X-M., Li, Y. & Ruan, W-J., 2019. *Pyrene-based MOFs as fluorescent sensor for PAHs: an energetic pathway of the backbone structure effect on response.* Dalton Transactions, 48(17), 5705-5712.
31. Yu, J., Park, JH., Wyk, A.V, Rumbles, G. & Deria, P., 2018. *Excited-State Electronic Properties in Zr-Based Metal-Organic Frameworks as a Function of a Topological Network.* Journal of the American Chemical Society, 140(33), 10488-10496.
32. Schmeisser, M., Puchta, R., Eldik, R.v, Illner, P. & Zahl, A., 2012. *Gutmann Donor and Acceptor Numbers for Ionic Liquids.* Chemistry - A European Journal, 18, 10969-10982.
33. Edinburgh Instruments, 2012. *What is Stokes Shift?* Available online.
34. Edinburgh Instruments, 2012. *What is a Jablonski Diagram?* Available online.
35. Najbar, J. & Mac, M., 1991. *Mechanisms of fluorescence quenching or aromatic molecules by potassium iodide and potassium bromide in methanol-ethanol solutions.* Journal of the Chemical Society, Faraday Transactions, 87(10), 1523-1529.
36. Adhikary, R., 2010. *Application of fluorescence spectroscopy: excited-state dynamics, food-safety, and disease diagnosis.* [PhD thesis]. Iowa State University.
37. Chupp, T.E., Fierlinger, P., Ramsey-Musolf, M.J. & Singh, J.T., 2019. *Electric dipole moments of atoms, molecules, nuclei and particles.* Reviews of Modern Physics, 87(10), 1523-1529.
38. Cotton, F.A., 1990. *Chemical Applications of Group Theory, 3rd Edition.* John Wiley & Sons.
39. Edmund Optics, 2020. *Introduction to Polarization.* Available online.
40. Edmund Optics, 2020. *Understanding Waveplates and Retarders.* Available online.
41. Wang, T.C., Kim, I.S., Martinson, A.B.F. & Vermeulen, N.A., 2015. *Scalable synthesis and post-modification of a mesoporous metal-organic framework called NU-1000.* Nature Protocols, 11(1), 149-162.